NTNU
Norwegian University of
Science and Technology

Modelling Failure Mechanisms in Subsea Equipment

Siri Kildal Hansen

Chemical Engineering and Biotechnology
Submission date: June 2016
Supervisor: Johannes Jäschke, IKP
Co-supervisor: Adriaen Verheyleweghen, IKP

Norwegian University of Science and Technology
Department of Chemical Engineering

Preface

This work was completed at the Department of Chemical Engineering (IKP) at the Norwegian University of Science and Technology during the summer of 2016. It is the final part of my M.Sc degree in Chemical Engineering .

I would like to thank my supervisor, Associate Professor Johannes Jäschke, for giving me the opportunity to work on this project, and for his invaluable guidance and encouragement. I would also like to thank my co-supervisor Adriaen Verheyleweghen for his help throughout the project.

I also wish to thank my family who has never stopped encouraging me and supporting me, and my friends who always make me smile.

I declare that this is an independent work according to the exam regulations of Norwegian University of Science and Technology.

Trondheim, June 23, 2016
Siri Kildal Hansen

Summary

The oil and gas industry is recently facing a challenge to increase the efficiency and reduce the costs. One way to reduce costs is to better optimize the maintenance strategy. By applying failure mechanism models it could be possible to predict equipment degradation rates and estimate the remaining equipment lifetime based on some controllable input parameters. The operation could then be optimized for maintenance, safety and cost, which would be beneficial for both the company and the environment.

A literature review was performed in order to get an overview of important failure mechanisms in subsea equipment and how they can be modelled. The main focus has been on sand erosion, but failure mechanisms such as corrosion, erosion-corrosion and mechanical wear have also been included. Finally a case study was performed to see how sand erosion failure models can be used to predict equipment degradation and the estimated lifetime of the equipment. A base case was simulated to see how the system behaved with respect to sand erosion, and a parameter study was done to see how different liquid and gas velocities could affect failure rates and estimated equipment lifetime.

It was found that the major failure mechanisms in subsea equipment are erosion, corrosion and mechanical wear. The case study showed that it is indeed possible to use failure mechanism models to predict equipment lifetime as a function of simple input parameters. The simulations appear to give reasonable results when compared to theory. However, there is uncertainty about the validity of some of the results from the parameter study because of deviation from expected behaviour. It is believed that this could be because parts of the model was extrapolated beyond its range of validation.

Sammendrag

Olje- og gassindustrien har i dag store utfordringer knyttet til effektivisering og redusering av kostnader. En måte å redusere kostnader på kan være å finne bedre måter å optimalisere vedlikeholdsstrategier på. Ved å anvende modeller av feilmekanismer kan det være mulig å predikere degraderingshastigheten til utstyret og estimere levetiden basert på kontrollerbare parametre. Driften kan da optimaliseres for vedlikehold, sikkerhet og kostnader, noe som er gunstig både for bedriften og miljøet.

Et litteraturstudie har blitt utført for å få en oversikt over viktige feilmekanismer i subsea-utstyr og hvordan de kan modelleres. Hovedfokuset har vært på erosjon, men feilmekanismer som korrosjon, erosjon-korrosjon og mekanisk slitasje har også blitt inkludert. Mot slutten ble et case-studie utført for å se hvordan modeller av erosjon kan brukes for å predikere degradering av utstyr og estimere utstyrets levetid. Først ble en grunnleggende case simulert for å se hvordan systemet oppførte seg med hensyn på erosjon. Til slutt ble et parameterstudie gjennomført for å se hvordan enkeltparametre kan påvirke degraderingshastigheter og estimert levetid på utstyr.

I litteraturstudiet ble det funnet ut at de største feilmekanismene i subsea utstyr er erosjon, korrosjon og mekanisk slitasje. Case-studiet viste at det er mulig å bruke modeller av feilmekanismer til å predikere levetid til utstyr som en funksjon av enkle inputparametre. Simuleringene later til å gi fornuftige resultater når de sammenlignes med det som kan forventes ut i fra teori. Det er usikkerhet rundt gyldigheten til noen av resultatene, da de avviker fra det som er forventet. En mulig grunn til dette avviket kan være at deler av modellen er ekstrapolert utenfor dens gitte gyldighetsområde.

Contents

List of Figures

List of Tables

List of symbols

A	-	Dimensionless parameter
A_g	m^2	Effective gallery area
A_i	-	Constants
A_{corr}	m^2	Area exposed to corrosion
A_{pipe}	m^2	Cross sectional area of pipe
A_t	m^2	Area exposed to erosion
B		Brinell hardness factor
C		Particle concentration
C_1	-	A coefficient
	-	Model geometry factor
C_2	-	Particle size and fluid density correction
C_{bO_2}	mol/m^3	Concentration of bulk O_2
C_{corr}	mm/year	Corrosion rate
C_{fO_2}	mol/m^3	Concentration of fluid O_2
C_D	-	Drag coefficient
C_P	J/ kg K	Heat capacity
C_s	-	Monotonic effective shear strain
C_{unit}	-	Conversion factor
CR	mm/year	Corrosion rate
D	-	A constant
	inches	Pipe diameter
	m	Pipe diameter
	m	Gap between choke gallery and choke body
	m^2/s	Diffusion mass coefficient
d_p	μm	Particle diameter
e	-	Dimensionless factor
fCO_2	bar	Fugacity of CO_2
E	N/mm^2	Young's modulus
	-	Entrainment fraction
ER	mm/year	Erosion rate
G	-	Particle size correction function
GF	-	Geometry factor
h	m	Weld height
$F(\alpha)$	-	Function for ductility
F_D	N	Drag force
F_g	-	Pressure effect factor
F_G	G	Gravity force

F_M	-	Material factor
F_P		Penetration factor
	N	Pressure gradient force
F_{pH}	-	pH factor
$F_{r/D}$		Elbow radius factor
F_S	-	Sand sharpness factor
F_{scale}	-	High temperature factor
F_V	N	Virtual mass force
H	MPa	Hardness
H	m	Height of gallery
H_{LF}		Liquid film holdup
H_{LLS}		Liquid slug holdup
K		Material erosion constant
K_{ab}	-	Abrasive wear coefficient
K_{ad}	-	Adhesive wear coefficient
K_c	Mpa·$m^{1/2}$	Fracture toughness
	-	Corrosive wear coefficient
K_C		Corrosion rate
K_E		Erosion rate
K_{EC}		Erosion-corrosion rate
K_f	-	Fatigue wear coefficient
k_m	m/s	Wall mass transfer coefficient
l_f	m	liquid film length
l_S	m	Slug length
L	mm	Sliding distance
	inches	Stagnation length
	m	Length of pipe
L_{ref}	inches	Reference length
m	kg	Mass of particle
m_p	kg/s	Mass rate of sand
M	kg/mol	Molecular mass
N_f	-	Critical number of cycles
n	-	A constant
	-	Number of electrons
pCO_2	bar	Partial pressure CO_2
P	psi	Material hardness
	bar	Pressure
pH	-	pH
pH_{sat}	-	pH when the solution is saturated
Q	m^3/s	Mass flow

r	-	Ratio of plastic work to total work
r_1	m	Amount of corrosion in a year
r_i	m	Inner diameter of the pipe
r_o	m	Outer diameter of the pipe
R	J/ K mol	Gas constant
r_c	-	Radius of curvature
Re_p	-	Particle Reynolds particle number
Re_L	-	Liquid Reynolds number
S_{dot}	kg/s	Rate of sand flow
S_m	-	Geometry constant
V	mm^3	Wear volume
T	K	Temperature
T_m	K	Melting point
T_{scale}	K	Scaling temperature
t	s	Time
u	m/s	Fluid velocity
V_0	m/s	Initial particle velocity
V_{char}		Characteristic fluid velocity
$V_{droplet}$	m/s	Droplet velocity
V_D	m/s	Drift velocity
V_e	ft/s	Critical erosion velocity
V_f	ft/s	Fluid velocity
	m/s	Fluid velocity
V_{film}	m/s	Velocity of the liquid film
$V_{G_{core}}$	m/s	Gas core velocity
V_{LLS}	m/s	Velocity of the slug
V_{SG}	m/s	Superficial gas velocity
V_{SL}	m/s	Superficial liquid velocity
W	N	Normal load
We	-	Modified Weber number
x	m	Distance from beginning of stagnation length to particle
$\dot{W}_p$	bbl/month	Sand production rate
	kg/day	Sand production rate
α	rad	Characteristic impact angle
α_3	-	Material constant
β	-	Dimensionless parameter
δ_{film}	m	Thickness of the film
θ	rad	Angle of abrasive
θ	degrees	Inclination angle

ϵ_f	-	Reversing fatigue component
γ	-	Shear strain
μ	-	Coefficient of friction
μ_f	kg/ms	Fluid viscosity
μ_g	kg/ms	Gas viscosity
μ_l	kg/ms	Liquid viscosity
μ_m	kg/ms	Mixture viscosity
ρ_m	lbs/ft^3	Mixture density
	kg/m^3	Mixture density
ρ_g	kg/m^3	Gas density
ρ_m	kg/m^3	Fluid density
λ_L	-	A factor

1 Introduction

1.1 Motivation

The oil and gas industry is the largest export industry in Norway today, with 114 billion cubic metres of oil and gas exported in 2015. It equals 40% of the the Norwegian export values [Norwegian Petroleum, 2015a]. The first production of oil and gas on the Norwegian Continental Shelf began on the Ekofisk field in 1971 [Ministry of Petroleum and Energy, 2013]. Since then, a lot has happened. New technologies have opened up the possibility to produce from fields that were not previously available, and the oil recovery rate in each field has increased significantly. Today, 82 fields are in production [Norwegian Petroleum, 2015b].

The recent drop in oil price has forced oil companies to reduce costs and increase the efficiency. One way to reduce costs is to better optimize the maintenance strategy. Performing maintenance in subsea environments can be challenging because of harsh environmental conditions. By applying failure mechanism models it could be possible to predict equipment degradation rates and estimate the remaining equipment lifetime based on some controllable input parameters.

1.2 Object

The aim of this master thesis is to provide an overview of important failure mechanisms in subsea equipment, and to apply failure mechanism models in a simple subsea production system. This is one of the first steps towards the long term goal of being able to incorporate safety and maintenance as a part of the system's control structure and optimization strategy.

1.3 Previous work

Process control and RAMS (Reliabiliy, Availability, Maintainability and Safety) are two fields which both are well developed. However, an effort to combine these fields to be able to incorporate process control in safety and maintenance strategies is yet to be made.

The principle of process control is to use controllable variables to counteract the effect of disturbances on output variables. It can be applied short term in the purpose of keeping the process stable and long term in the purpose of

minimizing costs and maximizing net profit. There are some simple elements of safety in this field, but not much compared to the RAMS-field.

RAMS is concerned with the reliability and safety of systems. Stochastic models are applied to optimize the maintenance and reduce costs and risk. However, these models are usually in the based on monitoring the health of the equipment instead of predicting the health. Because of this it is hard to apply these principles in long term process control and optimization.

A lot of research has been done in the field of failure mechanisms, especially when it comes to sand erosion and corrosion. Mostly the models are applied to single components and not multi-component systems. There are only a few efforts to combine failure models and applying it to systems.

1.4 Outline

A major part of this thesis was to perform a literature review. The findings from the literature review is presented in Section 2 to Section 4. The case study that was performed towards the end is presented in Section 5.

The outline of this thesis is as following: Section 2 describes how various subsea equipment functions and which failure mechanisms are commonly found in the equipment. In Section 3 various failure mechanisms are described, along with how they can be modelled. The failure mechanisms that are included are mechanical wear, sand erosion and corrosion. Section 4 presents some failure databases. Section 5 presents the case study and shows the results from the base case and parameter study. The results are discussed in Section 6. Finally, a conclusion and suggestions for further work is presented in Section 7. Additional information like tables and MATLAB scripts are attached in the Appendix.

2 Common subsea equipment

This thesis is about modelling failure mechanisms in subsea equipment, but to be able to do this it is necessary to know which equipment is commonly used and how they work. In this section, the different types of equipments commonly used in subsea production and processing are presented.

2.1 Equipment overview

Table 2.1 presents an overview of the most commonly used equipment in offshore oil and gas production and processing.

Table 2.1: An overview of the equipment commonly used in subsea production and processing.

Wellheads	
Pipelines	Production pipeline
	Heavy crude oil pipeline
	Hydrotransport pipeline
	Waste water pipeline
	Tailing pipeline
	Transmission pipeline
Valves	Choke valve
	Ball valve
	Gate valve
	Needle valve
	Check valve
	Relief valve
	Blow-out preventer
Manifolds	
Risers	
Umbilicals	
Jumpers	
Christmas trees	
Separators	
Compressors	Positive displacement compressor
	Dynamic compressor
Pumps	Positive displacement pump
	Kinetc pump
	Multiphase pump

2.2 Wellheads

A wellhead is a pressure-containing component at the top of an oil or gas well that gives the structural interface for operations such as testing, completion and drilling. If the wellhead is located on the platform or onshore, it is called a surface wellhead. It can also be located on the seabed, and in this case it is called a mudline wellhead or a subsea wellhead [Bai and Bai, 2012]. A general wellhead is illustrated in Figure 2.1.

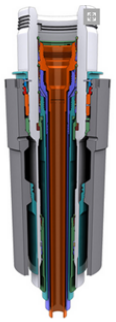

Figure 2.1: Illustration of wellhead [Oil & Gas Portal, nd]

The most common failure mechanisms in wellheads are *corrosion*, *erosion* and *fatigue wear* [Dale et al., 2013, Reinås, 2012].

2.3 Pipelines

Pipelines are used to transport material from one location to another by pressure differences provided by compressors and pumps. The subsea pipelines are designed to withstand conditions with high pressure and high temperature (HP/HT). The pressure in HP/HT pipelines ranges from 300-500 bar and the temperature is typically between 120-160°C [Rambøll, nd]. A typical subsea pipeline is illustrated in Figure 2.2.

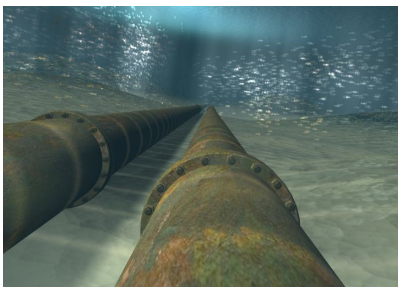

Figure 2.2: A typical pipeline located on the seabed [Subsea World News, 2013b].

Pipelines may be flexible or rigid. Rigid pipelines generally require a larger wall thickness to support a given load. They are usually made of materials such as concrete, clay, cast iron and asbestos. Rigid pipes are most commonly used for low pressure and gravity flow applications. Flexible pipelines are increasingly used in oil and gas production. They are usually made of materials such as steel, copper, plastic and ductile iron. Flexible pipelines allow for the soil beneath and on the sides of the pipeline to support some of the load, giving the pipelines a high effective strength. [Bai and Bai, 2012, Muhlbauer, 2004].

Pipelines are designed to transport different kinds of materials, and there are several types or pipelines. This include production pipelines, heavy crude oil pipelines, hydrotransport pipelines, waste water pipelines, tailing pipelines and transmission pipelines [Papavinasam, 2014].

Production pipelines
Production pipelines, or flowlines, transport crude oil and gas from the wellheads to the processing facilities. They usually start as rather small in diameter, and as the production pipelines from the different wellheads converge, the pipelines become larger [Papavinasam, 2014].

The most common failure mechanism in production pipelines is *corrosion* by CO_2 and H_2S. *Erosion* is also quite common at high velocities, and it is the bends and the tees that are most prone to erosion damage. Other prevalent failure mechanisms are *hydrogen induced cracking, stepwise cracking, sulfide stress cracking* and *hydrogen blistering*. The cold temperature can cause the pipe to be *plugged*, either because of *formation of hydrates* in gas pipelines or the *deposition of wax, asphaltenes* and *parafins* in oil pipelines [Papavinasam, 2014].

Heavy crude oil pipelines
Heavy crude oil pipelines are special production pipelines designed to transport crude oils with high wax contents or high pour points. The crude oil is heated before entering the pipeline to reduce its viscosity. The pipe is carefully insulated and heaters are installed along the pipeline to keep the temperature of the oil up to prevent *plugging* of the pipe. Heavy crude oil pipelines can experience *corrosion*, but it is usually less severe than in regular production pipelines [Papavinasam, 2014].

Hydrotransport pipelines
Hydrotransport pipelines are used to transport oilsands to the extraction facilities. Oilsand is mixed with water to form a slurry before it is transport along the pipeline. The most common failure mechanism in hydrotransport pipelines is *erosion*, due to the large amount of sand [Papavinasam, 2014].

Waste water pipelines
Waste water pipelines transport the waste water to a disposal facility. The waste water is a result from the separation of water from oil and gas. Most of the water is recycled, but a small portion of the water becomes waste. The waste water has to be treated to remove suspended oil and sand, scale, bacteria and acid gases. The dominant failure mechanism in water waste pipelines is *corrosion*, both internal and external [Papavinasam, 2014].

Tailing pipelines
Tailing pipelines, or slurry pipelines, is a type of waste water pipeline. They transport the mixture of clay, silts, sand and water that is left when the oil is removed from the oilsand to safe deposits. The most common failure mechanisms in tailing pipelines are *corrosion* and *erosion* [Papavinasam, 2014].

Transmission pipelines
Transmission pipelines are used to transport oil and gas over large distances. There are several advantages to transporting oil and gas by pipelines. The transportation cost and energy required to operate is less than other ways of transportation, such as railroads, trucks, airplanes and barges. It is also considered to be a safe and reliable method of transportation, and not as sensitive to inflation as other transportation methods [Papavinasam, 2014].

Gas transmission pipelines require the water content to be less than 7 lb/MMcf. If the separator for some reason does not work, water may enter the pipeline and increase the susceptibility to *corrosion*. Water will usually accumulate at the pipeline floor causing *corrosion* to happen here [Papavinasam, 2014].

Oil transmission pipelines transport crude oil from oil separators to tankers or refineries. The probability of erosion and corrosion is very low because most of the erosive and corrosive materials are removed upstream [Papavinasam, 2014].

2.4 Valves

Valves are used in processing to control the flow and pressure by opening, or closing the pathways of the flow A list of the most common valves used today is presented below.

- Choke valve
- Ball valve
- Gate valve
- Needle valve
- Check valve
- Relief valve
- Blow-out preventor

Common failure mechanisms in valves are *corrosion, erosion, mechanical failure, mechanical wea*r and *material defects* [Peters, 2003].

Choke valves are commonly used in the oil and gas industry as control and safety devices. A choke valve consists of an internal casing with holes. When the casing is rotated by an actuator, the position of the holes is altered and the fluid flow is modified. The fluid enters from the side and changes direction as it goes through the internal casing. An illustration of a choke valve is shown in Figure 2.3.

Figure 2.3: An image of a choke valve [In Line Valve, nd].

Ball valves are the most commonly used valves in the oil and gas industry. Inside a ball valve there is a ball that controls the flow. The ball has a hole going through it, and when this hole is in line with the flow, the valve is fully open. To close the valve, the ball is turned 90° by turning a handle. The valve is either fully open or fully closed, there is no intermediate position [Polyprocessing, nd]. An illustration of a ball valve is shown in Figure 2.4.

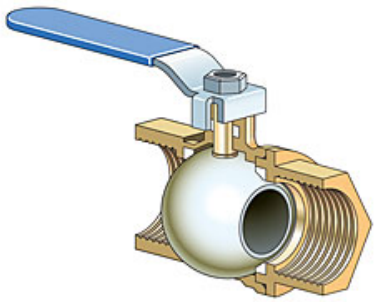

Figure 2.4: Illustration of a ball valve [Polyprocessing, nd].

Gate valves are opened by lifting a rectangular or round gate away from the path of the fluid. An illustration of a gate valve is shown in Figure 2.5.

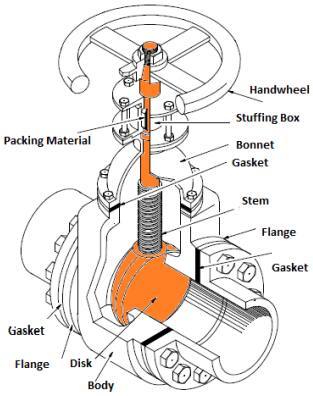

Figure 2.5: A gate valve [Polyprocessing, nd].

Needle valves are used for precise regulation of relatively low flow rates. They consist of a needle-like stem that fits perfectly to close off the flow from small diameter pipelines [Adkins, 2012]. An illustration of a needle valve is shown in Figure 2.6.

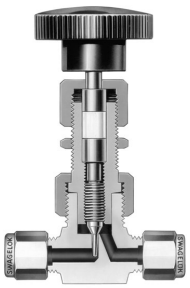

Figure 2.6: Illustration of a needle valve [Adkins, 2012].

Check valves are used to prevent backflow. During normal operation, a spring-loaded gate is pushed open, allowing for free fluid flow. In the case of backflow, the gate is forced into locked position [Adkins, 2012, Shorts, nd]. An illustration of a check valve is shown in Figure 2.7.

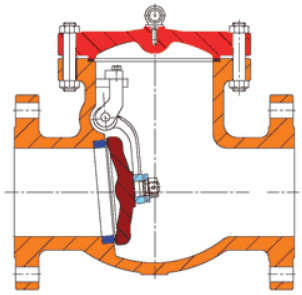

Figure 2.7: Illustration of a check valve [Shorts, nd].

Relief valves are used to control the pressure in a system. They contain a vent that opens to the atmosphere when the system pressure exceeds a certain limit. The vent closes again when the pressure returns below the limit [Adkins, 2012]. An illustration of a relief valve is shown in Figure 2.8.

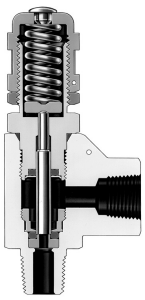

Figure 2.8: Illustration of a relief valve [Adkins, 2012].

A **Blowout preventer (BOP)** is a large valve designed to prevent blowout during drilling. It is closed if the operators lose control of formation fluids. An illustration of a blow out preventor is shown in Figure 2.9.

Figure 2.9: Illustration of a blowout preventer (BOP) [Sunnda Corporation, nd].

2.5 Manifolds

A manifold is an arrangement of pipes and/or valves used to monitor, control and distribute fluid flow. It is used to simplify the subsea system and optimize the fluid flow [Bai and Bai, 2012]. An illustration of a manifold is shown in Figure 2.10.

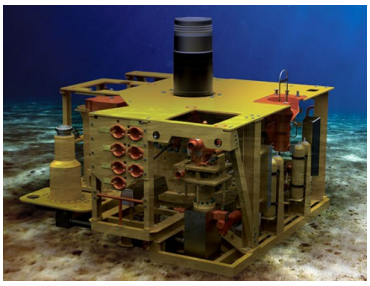

Figure 2.10: Illustration of a manifold [Subsea World News, 2013a]

Manifolds may range from small structures like PLEMs (pipeline end manifolds) to larger structures like subsea processing systems [Bai and Bai, 2012]. As manifolds consists of pipes and valves, the most common failure mechanisms in manifolds are considered to be the same as in pipes and valves: *corrosion, erosion, mechanical failure, mechanical wea*r and *material defects.*

2.6 Risers

A riser is a part of the flowline that transports material from the seabed to the production and drilling facilities at the surface of the sea. Figure 2.11 illustrates how multiple risers connect the ship to the seabed facilities.

The dimensions of a riser normally range between 3 and 12 inches, and the length depends on the water depth and riser configuration [Bai and Bai, 2012].

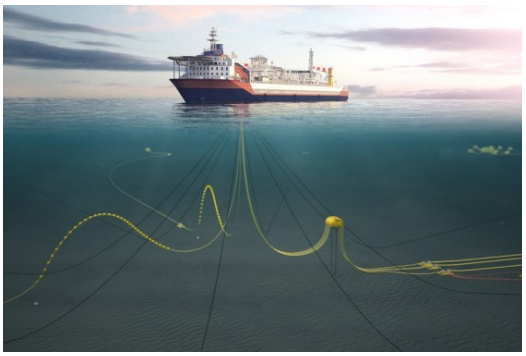

Figure 2.11: Multiple risers transporting materials from the seabed to the ship at the sea surface [4subsea, nd].

The major failure mechanisms of risers are the same as in pipes: *erosion* and *corrosion*.

2.7 Umbilicals

Umbilicals are important components in a subsea production system as they contain tubing, electrical cables, hydraulic lines, fibre optic cables and piping [DNV-GL, 2015a, Bai and Bai, 2012]. The components are protected by an outer shell. A typical umbilical is shown in Figure 2.12. Umbilicals make sure power, chemicals and communication is transferred to equipments such as valves, jumpers, sleds, trees and manifolds [Bai and Bai, 2012].

The dimensions of an umbilical normally range up to 25.4 cm and the tubing inside typically ranges up to 5.08 cm. The length of an umbilical depends on the spacing between the subsea components and their distance from the host facility [Bai and Bai, 2012].

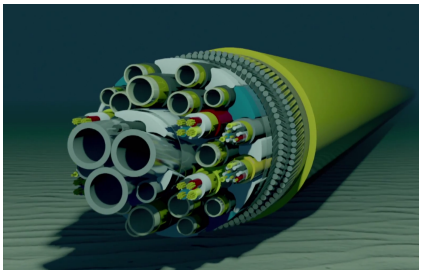

Figure 2.12: A subsea umbilical from the Alder field in the central North Sea [Subsea World News, 2014].

The major failure modes for steel tube umbilicals are *fatigue, corrosion, service loads* and *accidental damage* [Bai and Bai, 2005].

2.8 Jumpers

A jumper is a short pipe that is used to transport fluid between two components, for example a manifold and a tree, two manifolds or a sled and a manifold [Bai and Bai, 2012]. An image of a jumper is shown in Figure 2.13.

Figure 2.13: An image of a subsea jumper [Gulf Island Fabrication, nd]

The most common failure mechanisms in jumper are the same as for a pipe: *erosion* and *corrosion*.

2.9 Christmas trees

Christmas trees are located on top of the wellhead. They are a combination of valves, pipes, connections and fittings [Bai and Bai, 2012]. An illustration of a Christmas tree can be seen in Figure 2.14.

Figure 2.14: Illustration of a Christmas tree [Tipvalve Industrial Group, nd]

The major failure mechanisms in Christmas trees are the same as for valves and pipes: *corrosion, erosion, mechanical failure, mechanical wear* and *material defects.*

2.10 Separators

Separators are used to separate sand, water, gas and oil. The separators are designed as pressure vessels to be able to handle high flow rates. A common failure mechanism in separators is *corrosion* [Papavinasam, 2014].

Oil-gas separators
In an oil-gas separator the gas is separated from the oil. Oil gas separators normally consist of a section for primary separation, gravity settling and liquid settling, a mist extractor, oil outlet, gas outlet, water outlet, valves, motors and storage tanks [Papavinasam, 2014].

Paraffin may be deposited in the separator, and this may cause *blockage* of the fluid flow and and mist extractor. The *deposited paraffin* may be removed by flushing and washing, but it is preferred to avoid it by adding chemicals, heating the separation and coating the internal surface [Papavinasam, 2014].

Formation of foams may occur in the separator when the pressure is reduced. The foam is removed by heating, adding chemicals or using centrifugal force [Papavinasam, 2014].

Solids, salt and acid gases present in the mixture of oil-gas could cause *corrosion* in the separator. One problem is that some of the measures taken against paraffin deposition and foaming counteract the measures taken against corrosion, which makes this is an optimization problem [Papavinasam, 2014].

Oil-solid separator
Solids such as sand, rust and scales are separated by cyclones, gravity settling, filters, flotation methods and centrifuges [Papavinasam, 2014].

Oil-water separator
Stable oil-water emulsions may form, although this is unwanted and prevented to a high degree. Chemicals that give stable emulsions are avoided, as well as equipment like pumps, elbows and tees as they could cause mechanical dispersion [Papavinasam, 2014].

2.11 Compressors

Compressors are used to increase the pressure of the gas for the transportation through pipelines. There are mainly two types of compressors:

- Positive displacement compressors
- Dynamic (centrifugal) compressors

The most common failure mechanisms in compressors are *corrosion*, *erosion*, *fouling* and *mechanical wear* [Papavinasam, 2014].

Positive displacement compressors
Positive displacement compressors increase the pressure of the gas by enclosing it in a confined volume before reducing the volume of the gas. The compressed gas is then discharged. Positive displacement compressors can be divided into rotary compressors and reciprocating compressors [Papavinasam, 2014]. Both compressors are illustrated in Figure 2.15.

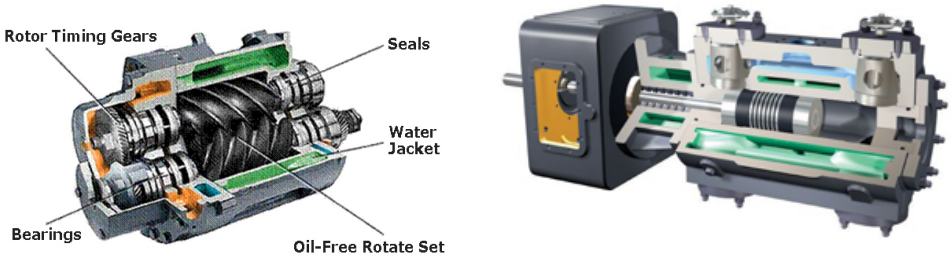

(a) Rotary compressor **(b)** Reciprocating compressor

Figure 2.15: Positive displacement compressors **(a)** A rotary compressor [Natural Resources Canada, nd]. **(b)** A reciprocating compressor [A & W Compressor, nd].

A rotary compressor is illustrated in Figure 2.15a. Rotary compressors have rotors equipped with lobes or vanes that traps the gas and pressurize it. A reciprocating compressor is illustrated in Figure 2.15b. The volume of the gas is reduced by a piston moving in a cylinder [Papavinasam, 2014].

Dynamic compressors
Dynamic compressors are also called centrifugal compressors. The pressure of the gas is increased by inertial forces, meaning that energy is used to increase the velocity. Dynamic compressors can be divided into axial and radial (centrifugal) compressors [Papavinasam, 2014]. Both compressors are illustrated in Figure 2.16.

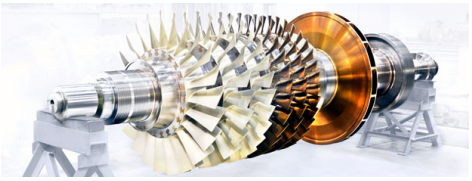

(a) Axial compressor

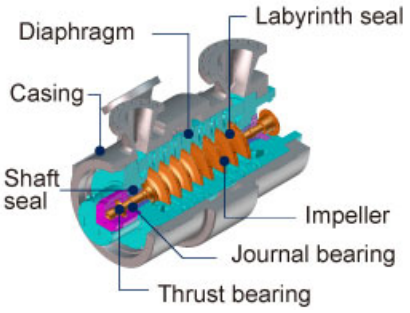

(b) Radial compressor

Figure 2.16: Illustration of dynamic compressors. **(a)** Illustration of an axial compressor [MAN Turbomachinery, nd]. **(b)** Radial (centrifugal) compressor [MHI Compressor Corporation, nd].

In axial compressors the gas flows parallel to the axis of rotation. An illustration of an axial compressor is shown in Figure 2.16a. The direction of the gas is not changed in axial compressors, while this is not the case in centrifugal compressors. Centrifugal compressors increase the velocity by the blades on a rotating impeller. An illustration of a centrifugal compressor is shown in Figure 2.16b.

2.12 Pumps

Pumps generate pressure so that liquids can be transported through pipelines. There are two types of pumps: positive displacement pumps and kinetic pumps. Common failure mechanisms in pumps are *erosion, corrosion, cavitation* and *mechanical wear*.

Positive displacement pumps

Positive displacement pumps use gears, pistons and diaphragms to pressurize the fluid. They can be divided into rotary and reciprocating pumps. Reciprocating pumps use pistons or cranks to increase the pressure of the liquid, while rotary pumps trap the liquid and displace it in each rotating turn. Rotary pumps work differently depending on the type of rotary pump. An illustration of a positive displacement pump can be seen in Figure 2.17.

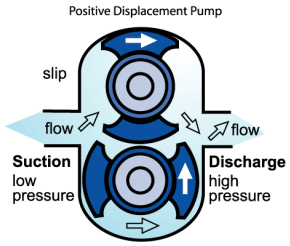

Figure 2.17: Illustration of a positive displacement pump [IEEE Globalspec, nd]

Kinetic pumps

Kinetic pumps can be divided into peripheral and centrifugal. The most commonly used pump in oil transmission pipelines is the centrifugal pump. They are powered by electric motors or internal combustion engines and can handle big volumes. Rotational kinetic energy is transformed to hydrodynamic energy in the fluid [Papavinasam, 2014]. An illustration of a centrifugal pump is shown in Figure 2.18.

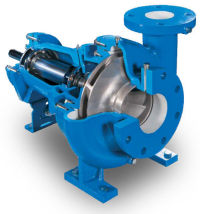

Figure 2.18: Illustration of a centrifugal pump [Febo and Paganini, 2016]

Multiphase pumps

Multiphase pumps are becoming more common in subsea production and processing. Traditional pumps are only able to pump liquid flow. To transport oil and gas you typically need a scrubber to separate the oil from the gas, a compressor to transport the gas and a pump to transport the oil. However, multiphase pumps are able to handle flow with high contents of gas, thus only the multiphase pump is needed to transport the oil and gas [Liu, 2015].

3 Failure mechanisms

This section provides an overview of the different failure mechanisms that have been discovered during the literature study. Failure mechanisms connected to electrical failures and signal failures have not been considered, in addition to failures during transportation and installation. Failures caused by human error, natural disasters and the weather is not included either. These failure mechanisms have not been included in this thesis, because they are not generally something that can be controlled. They are therefore not very relevant with respect to process control.

Many failure mechanisms have not been included in this section because of a need to limit the scope of the thesis. A list of the failure mechanisms discovered is provided below.

- Mechanical wear (adhesion, abrasion, fatigue wear and corrosive wear)
- Sand erosion
- Corrosion
- Cavitation erosion
- Droplet erosion
- Flashing
- Fouling
- Equipment plugging
- Cracking
- Crack propagation
- Formation of foams
- Deposition of wax, asphaltenes and parafins
- Vortex-induced vibrations
- Material defects
- Mechanical failure
- Marine growth

The most common failure mechanisms are mechanical wear, sand erosion and corrosion. These failure mechanisms have been presented in this section.

Considering this is an overview of the different failure mechanisms, it is in no way a complete review of them. Multiple master theses could be written about each topic, and for thorough information about a mechanism it is recommended to take a look in the literature cited, as well as other sources.

3.1 Mechanical wear

Wear is the mechanism where material is removed from a surface because of contact with another surface. It is a common failure mechanism in equipment with moving parts such as pumps, compressors and valves. It can happen because of microfractures, melting at the interface or chemical dissolution. Almost all machines have reduced reliability because of wear issues, which makes this failure mechanism very important. There are several types of wear mechanisms:

- Adhesive wear
- Abrasive wear
- Fatigue wear
- Corrosive wear

These are the very basic wear mechanism and they can also be recognized in failure mechanisms such as sand erosion and corrosion.

The dominant wear mechanism in a system can change depending on changes in factors like chemical film formation and surface material properties. Usually wear does not happen through only one wear mechanism, but as a combination of multiple mechanisms [Bhushan, 2000].

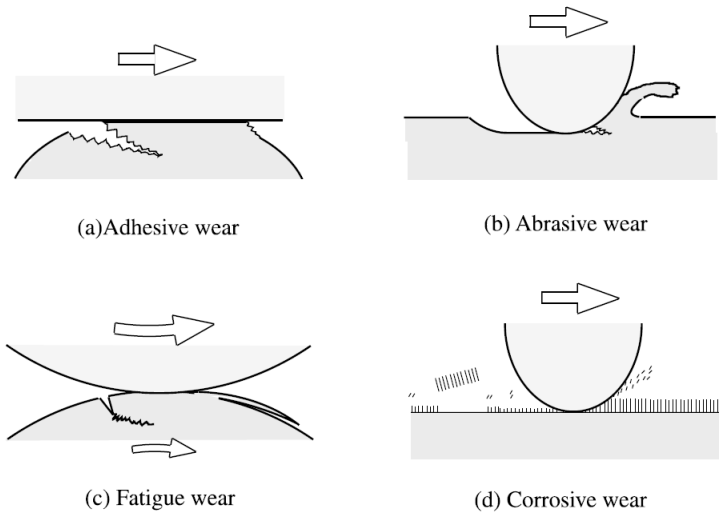

Figure 3.1: An illustration of the four wear mechanisms described in this section: adhesion, abrasion, fatigue wear and corrosive wear [Bhushan, 2000]

Equations to calculate the wear volume because of mechanical wear are given for each wear mechanism. They are very general and could be a good basis for deriving mechanistic failure models for other failure mechanisms.

3.1.1 Adhesive wear

Adhesive wear is caused by large plastic deformation in the contact region because of strong adhesive bonding between two surfaces. This leads to crack formation and propagation. Wear particles are formed once the crack reaches the contact surface [Bhushan, 2000]. The general mechanism is illustrated in Figure 3.2.

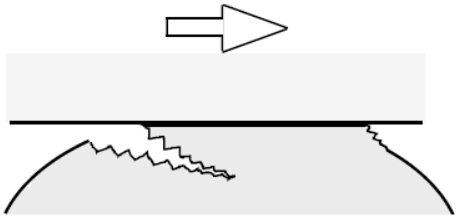

Figure 3.2: Adhesion mechanism: contact between two surfaces causes crack formation and propagation. Once the crack reaches the surface, wear particles are formed [Bhushan, 2000].

The wear volume V is given by:

$$V = \frac{1}{3} \cdot \frac{WL}{H} \tag{3.1}$$

where W is the normal load, L is the sliding distance and H is the hardness of the material. However, there are various wear particle modes (such as flake-like wear particle and wedge-like particle) and the particles are not only created in the soft material. To be able to take these factors into account as well some others, an adhesive wear coefficient K_{ad} is introduced:

$$V = K_{ad} \cdot \frac{WL}{H} \tag{3.2}$$

The adhesive wear coefficient is not necessarily a constant value, but it depends upon the operating conditions [Bhushan, 2000].

3.1.2 Abrasive wear

Abrasion is the wear mechanism where sliding and ploughing remove a part of the surface material of the weakest material to form a groove in the surface. The abrasion mechanism is illustrated in Figure 3.3.

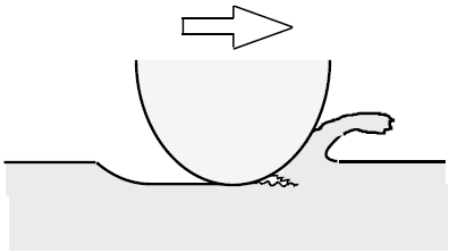

Figure 3.3: Abrasion mechanism: sliding and ploughing remove a part of the surface material and forms a groove [Bhushan, 2000].

The abrasion mechanism is somewhat different in ductile and brittle materials. There are three main abrasion modes: cutting, wedge-forming and ploughing, as can be seen from Figure 3.4 [Bhushan, 2000].

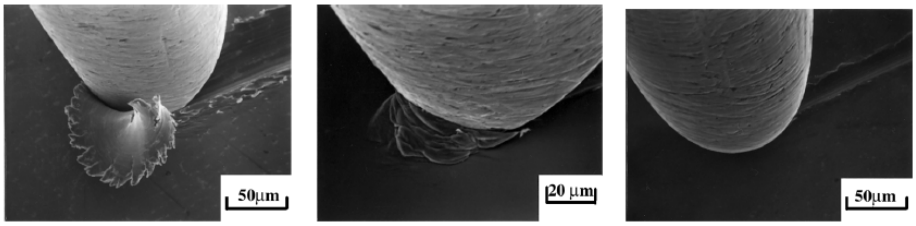

Figure 3.4: Using SEM to observe the three different failure modes in abrasive wear: **(a)** cutting mode, **(b)** wedge-forming mode and **(c)** ploughing mode [Bhushan, 2000].

Abrasive wear in ductile materials
In ductile materials, long wear particles are generated by microcutting. The wear volume for the abrasive grooving in microcutting can be found from the following equation:

$$V = \frac{2}{\pi \cdot \tan\theta} \cdot \frac{WL}{H} \tag{3.3}$$

where θ is the angle of the assumed conical abrasive, W is the normal load, L is the sliding distance and H is the hardness of the wearing material. To take into account the other two abrasion modes, the parameter K_{ab} is introduced [Bhushan, 2000]:

$$V = K_{ab} \cdot \frac{WL}{H} \tag{3.4}$$

Abrasive wear in brittle materials
In brittle materials, wear particles are generated by crack propagation. Because of this, the wear rate is dependent on the fracture toughness of the material. The abrasive wear volume in brittle materials can be found from the following equation:

$$V = \alpha_3 \frac{W^{9/8}}{K_c^{1/2} H^{5/8}} \left(\frac{E}{H}\right)^{4/5} L \tag{3.5}$$

where α_3 is a material constant determined by calibration, W is the normal load, K_c is the fracture toughness, H is the hardness, E is Young's modulus and L is the sliding distance [Bhushan, 2000].

3.1.3 Fatigue wear

Adhesive and abrasive wear are not dependent on the number of contacts for the generation of wear particles. However, in some cases the number of

contact cycles is important for the formation of wear particles. This is called fatigue wear. Fatigue wear is caused by a certain number of repeated contacts between surfaces. The mechanism is considered a high-fatigue mechanism if the number of contact cycles is high. If the number of contact cycles is low, it is considered a low-cycle fatigue mechanism [Bhushan, 2000]. The general mechanism of fatigue wear is illustrated in Figure 3.5.

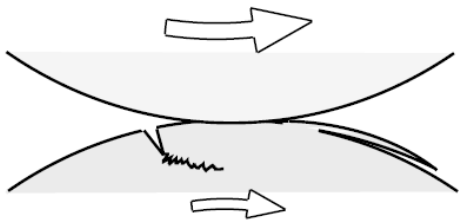

Figure 3.5: Fatigue wear mechanism: cracks are generated after certain number of cycles [Bhushan, 2000].

Elastic contact

Elastic contact is usually observed in rolling components, which is used in compressors and centrifugal pumps. The main mechanism in this case is high-cycle fatigue failure in the contact region. The critical number of rolling cycles N_f is experimentally determined to be

$$N_f \propto \frac{1}{W^n} \tag{3.6}$$

where W is the normal load and n is a constant depending on the rolling element shape. This equation is commonly used for fatigue wear in rolling bearings, which can be found in compressors, where $n = 3$ [Bhushan, 2000].

Plastic contact

It is possible that when two surfaces have contact no wear particles are formed, but instead a groove is formed at the path of contact. This is called ploughing. After a critical number of cycles, this ploughing is expected to cause a fatigue fracture. After repeated friction on the surface, a surface layer is gradually peeled off with increasing number of cycles [Bhushan, 2000].

If the layer is assumed to be detached from the surface as wear particles, the critical number of cycles is given by a modification of the Coffin-Manson relationship:

$$N_f = \left(\frac{C_s}{\Delta\gamma_s}\right)^D \tag{3.7}$$

where C_s is the monotonic effective shear strain, D is a constant in the range of 2-3, and $\Delta\gamma_s$ the effective shear strain increment per wave pass and D is a constant (usually 2). The wear volume can be found from the following equation:

$$V = K_f \cdot \frac{WL}{H} \tag{3.8}$$

where K_f is the fatigue wear constant, W is the normal load, L is the sliding distance and H is the hardness of the material. The fatigue wear constant can be determined from the following equation:

$$K_f = \frac{3 \times 3^{1/2} r\mu}{C_S^D \Delta\gamma_s^{1-D}} \tag{3.9}$$

where r is the ratio of plastic work to total work and μ is the coefficient of friction for the contacting surfaces [Challen et al., 1986].

There are two other modes of abrasive wear: ratcheting and cyclic plasticity. In ratcheting, shear strain per cycle is accumulated until it reaches a critical value C and a surface failure occurs. The number of cycles to failure can then be found from the following equation:

$$N_r = \left(\frac{C}{\Delta\gamma_r}\right) \tag{3.10}$$

where γ_r is the shear strain of ratcheting per cycle [Bhushan, 2000].

In cyclic plasticity, a cyclic axial plastic strain acts parallel to the surface. The critical number of cycles is given by the Coffin-Madison relationship:

$$N_f = \left(\frac{2C}{\Delta\epsilon_f}\right)^{1/n} \tag{3.11}$$

where C is the monotonic fracture strand, $\Delta\epsilon_f$ is a reversing fatigue component due to the axial plastic strain and $n \approx 0.5$ [Johnson, 1995].

It is reasonable to assume that all fatigue failures modes may coexist, and which fatigue failure is the dominating one will depend on the contact condition [Bhushan, 2000].

3.1.4 Corrosive wear

Chemical and electrochemical reactions may occur on the material surface. The mechanism of corrosion is described in detail in Section 3.3. If the

reaction product from corrosion is similar to the surface material, this may not be a big issue. In this case the wear mechanism will mostly be the same as for the bulk material. However, often the surface material is different from the bulk material, and in this case the wear mechanism is quite different. The reaction product forms a layer on top of the bulk material, which is removed by friction. Therefore, the growth rate of the reaction layer is important for the calculation of wear volume. The general mechanism of corrosive wear is illustrated in Figure 3.6.

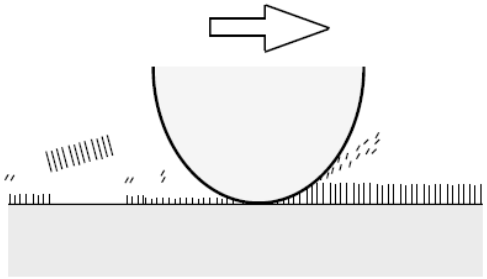

Figure 3.6: Corrosive wear mechanism: a reaction layer is formed from tribo-chemical reactions, and later removed by friction [Bhushan, 2000].

The oxidative wear volume can be estimated with the following equation:

$$V = K_c \frac{WL}{H} \tag{3.12}$$

where K_c is the corrosive wear coefficient, W is the normal load, L is the sliding distance and H is the hardness of the material. K_c is a constant depending on factors like Arrhenius' constant, density of the material, sliding velocity, activation energy and temperature [Bhushan, 2000].

The mechanism of corrosion is further described in Section 3.3.

3.2 Sand erosion

Production of sand is very common during oil and gas production, and can cause pipe blockage, pressure drop and erosion. This is a big problem within the oil and gas industry, as it causes both financial and environmental issues [Parsi et al., 2014]. Sand erosion damage in a pipe bend and choke valve is shown in Figure 3.7.

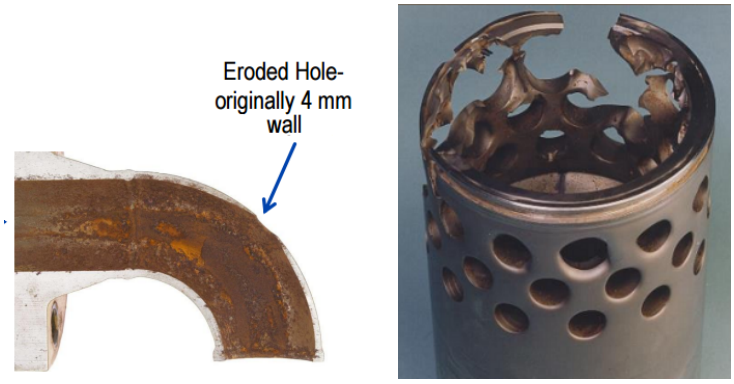

(a) (b)

Figure 3.7: Sand erosion damage in pipeline bends and a choke valve [Peters, 2014]. **(a)** Sand erosion in a 50 mm pipeline bend. **(b)** Sand erosion in a choke valve part.

Sand erosion can cause damage in many types of equipment. In a review document by Barton the following list was presented to rank the components most vunerable to erosion [Barton, 2003]:

1. Chokes
2. Sudden constrictions
3. Partially closed valves
4. Standard radius elbows
5. Weld intrusions
6. Reducers
7. Long radius elbows
8. Blind tees
9. Straight pipes

Sand screens and gravel packs are often used to prevent sand erosion, but they are not always effective. Sand screens can only keep particles larger than 50 μm from entering the system, meaning that smaller particles move freely into the system. The small particles can also block parts of the screen, making the openings bigger due to larger velocity and erosion in other areas of the screen. Thus, larger particles may also enter the system [Parsi et al., 2014]. The equipment is also usually coated with an erosion-resistance coating to prevent erosion.

3.2.1 The mechanism of sand erosion

The mechanism of erosion is believed to be somewhat different in ductile and brittle materials [Parsi et al., 2014].

The erosion in brittle materials is caused by crack formation when the particle hits the surface. The creation of radial and lateral cracks divides the surface into tiny pieces. When other particles hit the surface, the cracks are deepened or small pieces of the wall are removed [Parsi et al., 2014]. An illustration of the erosion mechanism in brittle material is shown in Figure 3.8. Similarities to the adhesion mechanism described in Section 3.1.1 can be seen.

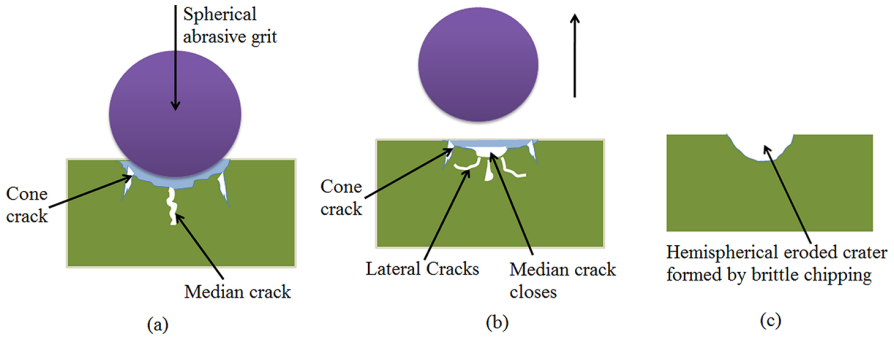

Figure 3.8: Suggested erosion mechanism in brittle materials [Sooraj and Radhakrishnan, 2013]. **(a)** Cone cracks and median cracks are formed. **(b)** Median cracks are closed and laterial cracks are formed. **(c)** An eroded crater is formed.

Several sand erosion mechanisms have been suggested for ductile materials. Finnie suggested that the erosion is a result of micro-cutting. A crater is formed and the peeled off material is piled up around the crater, which is removed after more particle impacts [Finnie, 1960]. This mechanism is illustrated in Figure 3.9. Similarities to the abrasion mechanism described in Section 3.1.2 can be seen.

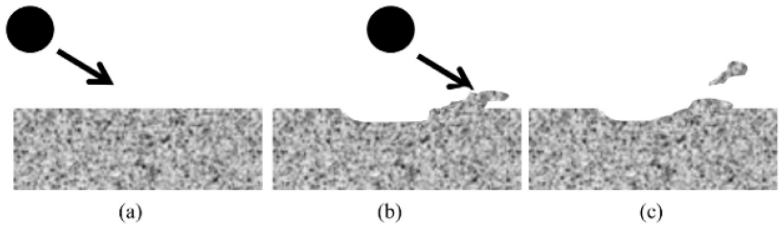

Figure 3.9: Suggested erosion mechanism in ductile materials by Finnie taken from the erosion review by Parsi et al. [Parsi et al., 2014]. **(a)** The particle hits the surface material. **(b)** A crater is formed and excess material is piled up around it. **(c)** The piled up material is removed by further particle impacts.

A macroscopic erosion mechanism for ductile materials has been suggested by Bellmann and Levy, where craters and platelets are created when particles hit the surface material. The platelets are removed from the surface once more particles impact the surface [Bellman and Levy, 1981].

3.2.2 Important sand erosion parameters

There are many parameters used in the modelling of sand erosion. A complete list of these parameters can be found in table A.1 in Apendix A.1. The most common parameters are particle size, particle shape, particle impact velocity, particle impact angle, particle material and fluid properties [Parsi et al., 2014].

Particle size has been observed to have a big influence on the magnitude of erosion. If two particles with the same velocity hit a wall, the larger particle will have the highest kinetic energy, hence do the greatest damage on the wall. Gandhi and Borse observed a linear relationship between sand particle size and erosion rate [Gandhi and Borse, 2002]. However, this model appeared to be not quite correct for all materials and velocities. Desale proposed the following relationship between particle size and erosion rate:

$$\text{Erosion rate} \propto \text{particle size}^n \tag{3.13}$$

where n is a constant that depends on the material, particle velocity and also particle size. It is usually in the range of 0.3 - 2.0. Often $n = 1$ is used, which gives the same result as Gandhi and Borse [Desale et al., 2009].

Particle shape has a great effect on the magnitude of erosion, and because of this a particle shape factor is often included in erosion rate equations. Sharper particles are more erosive than rounded or semi-rounded particles.

Salik and Buckley found that the erosion rate of crushed glass is a magnitude higher than the erosion rate for glass beads, definitely making this an important parameter [Salik and Buckley, 1981].

Particle impact velocity has a big effect on the erosion rate. Higher impact velocities give higher kinetic energy at the moment of impact, which gives higher erosion rates. The following equation is often used to describe the relationship between particle impact velocity and erosion rate:

$$\text{Erosion rate} \propto \text{particle impact velocity}^{n} \tag{3.14}$$

where n is a constant that is usually in the range of 1.6 to 2.6, but variations from 0.3 to 4 have also been observed [Parsi et al., 2014].

Particle impact angle is known to have a great effect on erosion rates. The effect depends on the surface material. In Figure 3.10 the effect of the impact angle on erosion rate in brittle and ductile materials is shown. As can be seen from the figure, the erosion rate in brittle materials increase as the angle approaches 90°, while in ductile materials the greatest impact angle seem to be located between 15-45°.

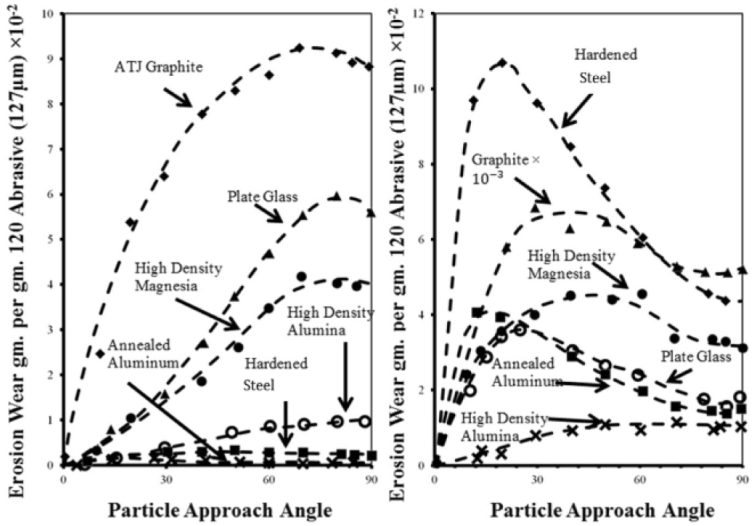

Figure 3.10: Erosion rate in brittle and ductile materials as a function of the particle impact angle. Brittle materials have an erosion rate peak at approximately 90° while ductile materials have a peak between 15-45° [Parsi et al., 2014].

Particle material is also a factor that is important when it comes to erosion rates. As can be seen in Figure 3.10, different materials give different erosion

rates. This is due to material properties such as hardness and density. In general, particles with higher density have higher kinetic energy and thus cause higher erosion rates [Parsi et al., 2014]. As for material hardness, the erosion rate increases with increasing material hardness, the hardness of the target wall is also essential. The following relationship has been suggested by Wada and Watanabe:

$$\text{Erosion rate} \propto \left(\frac{\text{Hardness of target material}}{\text{Hardness of particle}} \right)^n \tag{3.15}$$

where n is an empirical constant [Wada and Watanabe, 1987].

Fluid properties are important for the erosion rates because they affect the fluid flow and thus the particle velocity. For example, highly viscous fluids may slow the particle down, and turbulent flow may change the direction of the particle and throw it towards the wall. Fluid properties may also affect the local particle concentration. The local particle concentration may be high despite of low overall particle concentration due to flow pattern effects. This could give a higher erosion rate [Parsi et al., 2014].

3.2.3 Modelling sand erosion in pipelines

A lot of research has been done in the field of sand erosion, due to this being such a big issue in the oil and gas industry. As a result, a great amount of models have been suggested. The models are empirical, mechanistic, computational fluid dynamics (CFD) based, or a mix of these.

There are several models for estimating sand erosion in pipelines. Some of the models are presented in this section. The main areas for pipeline erosion are the elbows and tees, but reducers, welded joints and straight pipes may experience erosive damage as well.

American Petroleum Insititue Recommended Practice 14E (1991)
This is an empirical model used to estimate the erosion rate, developed by the Americal Petroleum Institute. The velocity where erosion may occur, V_e, in ft/s can be determined from the following equation:

$$V_e = \frac{C_1}{\sqrt{\rho_m}} \tag{3.16}$$

C_1 is an empirical constant (100 for continuous services and 125 for intermittent services) and ρ_m is the mixture density in lbs /ft^3 [American Petroleum

Institute, 1991].

The advantage of this model is that it very simple to apply, but it has received a lot of criticism for having several limitations. Important factors such as particle velocity, particle size, particle shape and multi-phase characteristics are not taken into account. It is not quite clear what this model is actually based on. It is also not physically correct. According to this model, increasing the density of the particle will lower the velocity of which erosion occurs. This is contrary to what was said about the relationship between density and erosion rate earlier in this section. When the density increase the erosion will occur at higher rates, thus V_e should increase as well [Parsi et al., 2014].

Model by Salama and Venkatesh (1983)
The model by Salama and Venkatesh is an empirical model to predict the erosion rate in ductile materials. The erosion rate, ER, in mils per year (mpy) can be determined from the following equation:

$$ER = 1.86 \cdot 10^5 \cdot \frac{\dot{W}_p}{P} \cdot \frac{V_f^2}{D^2} \tag{3.17}$$

where $\dot{W}_p$ is the sand production rate in bbl/month, P is the material hardness in psi, V_f is the fluid velocity in ft/s and D is the pipe diameter in inches [Salama and Venkatesh, 1983].

This model is more complex than the API RP 14E model and includes many of the significant parameters in sand erosion modelling. However, it does not take into account multi-phase flow [Salama and Venkatesh, 1983]. It is based on data from a sand-air system, so it is most accurate for gas flows. The experimental data used to develop and validate the model is presented in Table 3.2.

Table 3.2: The experimental values which the model by Salama and Venkatesh (1983) is based upon and validated against [Salama and Venkatesh, 1983].

Parameter	Symbol	Experimental range
Diameter	D	2 inches
Hardness	P	$1.55 \cdot 10^5$ psi
Velocity	V_f	50-100 ft/s
Sand flow rate	$\dot{W}_p$	86.62-144.37 bbl/month

Model by Salama (2000)
In an updated model from 2000, Salama includes particle diameter as well as fluid mixture density to take into account multi-phase flows. The new equation to determine the erosion rate, ER, in mm/year is as following:

$$ER = \frac{1}{S_m} \frac{\dot{W}_p V_m^2 d_p}{D^2 \rho_m} \tag{3.18}$$

where $\dot{W}_p$ is the sand production rate in kg/day, V_m is the mixture velocity of the fluid in m/s, d_p is the particle diameter in μm, D is the pipe diameter in mm and ρ_m is the mixture density in kg/m^3. S_m is a constant depending on geometry. For elbows it is 5.5, for tees with gas-liquid flow it is 68 and for tees with gas flow only it is 1379.
The data used for developing this model was almost exclusively taken from a liquid (water) and gas (nitrogen and air) systems, which means that the effect of fluid viscosity when the fluid density is the same has not been considered [Salama, 2000]. This model is based and validated against the data presented in Table 3.3.

Table 3.3: The experimental values which the model by Salama (2000) is based upon and validated against [Salama, 2000].

Parameter	Symbol	Experimental range
Gas velocity	V_g	0-222 m/s
Liquid velocity	V_l	0-11.49 m/s
Mixture velocity	V_m	7.5-222 m/s
Mixture density	ρ_m	1.20-1100.00 kg/m^3
Particle diameter	d_p	150-300 μm
Pipe diameter	D	26.5-52.5 mm
Geometry constant	S_m	5.5-1379

A problematic aspect in all of these empirical models is that there is great uncertainty connected to extrapolation. Different conditions may give other erosion mechanisms, and the model is only suited for the range of input values that were used to create it in the first place. When conditions change, the model may not be valid anymore. To battle this problem, scientist have suggested models based on erosion mechanisms and physics, including different parameters that may affect the erosion rate.

Model by Shirazi et al. (1995)
The model by Shirazi et al. is a mechanical/empirical model. Mechanical calculations are used to find the impact velocity of the particle, while empirical models are used to find the erosion rate in tees and elbows based on the impact velocity. The model consists of four steps:

1. Determine stagnation length
2. Determine flow velocity profile
3. Determine particle impact velocity
4. Determine erosion rate

A particle in a fluid moving towards a wall will at some point enter the stagnation region where it is decelerated. An illustration of where the stagnation region in tees and elbows is located can be found in Figure 3.11. If the particle is heavy and has a large momentum it will flow pass the stagnation region and impact the wall. On the other hand, if the particle is very light or moving in a more viscous flow, it may not hit the wall at all [Shirazi et al., 1995].

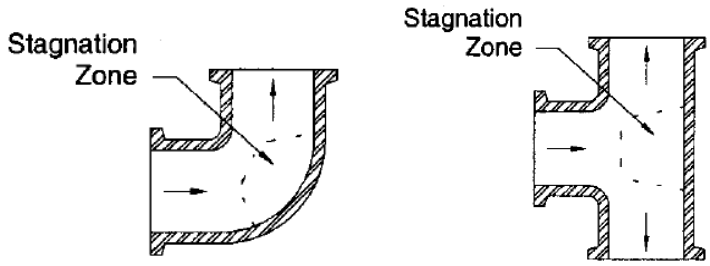

Figure 3.11: The stagnation region in elbows and tees [McLaury and Shirazi, 2000]. **(a)** The stagnation region in an elbow. **(b)** The stagnation region of a tee.

The stagnation length for tees can be found from the following equation:

$$\frac{L}{L_{ref}} = 1.35 - 1.32\tan^{-1}(1.63D^{-2.96}) + D^{0.247} \tag{3.19}$$

and the stagnation length for elbows can be obtained from the following equation:

$$\frac{L}{L_{ref}} = 1 - 1.27\tan^{-1}(1.01D^{-1.89}) + D^{0.129} \tag{3.20}$$

where D is the diameter of the pipe in inches and L_{ref} equals 1.06 inches. These are both semi-empirical equations [Shirazi et al., 1995].

To find the particle velocity it is necessary to know how the flow behaves in the stagnation region. It is assumed that flow velocity decreases from the initial velocity V_0 at $x = 0$ to 0 at $x = L$ (the wall), which gives the following fluid velocity profile:

$$V_f = V_0(1 - x/L) \tag{3.21}$$

where x is distance from the beginning of the stagnation region to the wall.

The velocity of the particle at the moment of impact is important for the magnitude of erosion. To find the particle impact velocity it is necessary to find the particle equation of motion. This is found from Newton's 2. law and the assumption that only the drag force is affecting the particle. The particle equation of motion is the following:

$$mV_p\frac{dV_p}{dx} = 0.5\rho_f(V_f - V_p)|V_f - V_p|C_D\frac{\pi d_p^2}{4} \tag{3.22}$$

where m is the mass of particle, V_p is the particle velocity, ρ_f is the fluid density, V_f is the fluid velocity, C_D is the drag coefficient and d_p is the particle diameter. Equation 3.22 is properly derived in Appendix B.

The drag coefficient, C_D can be expressed by:

$$C_D = \frac{24}{\mathrm{Re}_p} + 0.5 \tag{3.23}$$

where Re_p is the particle Reynolds number, given by:

$$\mathrm{Re}_p = \frac{\rho_f|V_f - V_p|d_p}{\mu_f} \tag{3.24}$$

where μ_f is the fluid viscosity [Shirazi et al., 1995].

To get a differential equation that is easier to solve, the following dimensionless variables are introduced:

$$\tilde{V}_p = V_p/V_0 \tag{3.25}$$

$$\tilde{V}_f = V_f/V_0 \tag{3.26}$$

$$\tilde{x} = x/L \tag{3.27}$$

Substituting the dimensionless variables and the drag coefficient term into Equation (3.22) gives the following differential equation:

$$\frac{d\tilde{V}_p}{d\tilde{x}} = \frac{3}{4}\left(\frac{L}{d_p}\right)\left(\frac{\rho_f}{\rho_p}\right)\left[\frac{24\mu_f(\tilde{V}_f - \tilde{V}_p)}{\tilde{V}_p V_0 d_p \rho_f} + \frac{0.5(\tilde{V}_f - \tilde{V}_p)|\tilde{V}_f - \tilde{V}_p|}{\tilde{V}_p}\right] \tag{3.28}$$

which can be solved numerically [Shirazi et al., 1995].

The particle impact velocity, V_L, equals the particle velocity, V_p, at $x = L$:

$$V_L = V_p(x = L) \tag{3.29}$$

The erosion ratio (ratio of mass removed from the target material to the mass of particle) can be found from the following empirical equation:

$$ER = 1.73 \cdot 10^{-6} V_L^{1.623} \tag{3.30}$$

The erosion rate is then estimated from the following equation:

$$E_{dot} = ER \cdot F_S \cdot S_{dot} \tag{3.31}$$

where F_S is the sand sharpness factor ranging from 0.2 in spherical particles to 1.0 for sharp-cornered sand and S_{dot} is the rate of sand flow in kg/s . [Shirazi et al., 1995].

The advantage of this model is that it accounts for many of the important sand erosion parameters, such as particle impact velocity, particle size, particle shape, particle density, fluid velocity, fluid density, fluid viscosity and the geometry of the target. The model predictions have been compared to actual experimental data with good results. The limitation of this model is that it is assumed that the particle travels in a straight line, which is not always the case. The effect of turbulence on particle trajectories and multi-phase flows are not taken into account either.

This model has been based upon and validated against the experimental parameters in Table 3.4.

Table 3.4: The experimental values in which the model by Shirazi (1995) is based upon and validated against [Shirazi et al., 1995].

Parameter	Symbol	Experimental range
Gas velocity	V_{SL}	0 - 12.8 m/s
Liquid velocity	V_{SG}	0 - 111 m/s
Sand velocity	S_{dot}/ρ_p	5.75 $\cdot 10^{-4}$ - 2.08 $\cdot 10^{-3}$ m^3/s
Radius of curvature	r_c	1.5 - 3.25

Model by McLaury and Shirazi (2000)
Modelling sand erosion in multi-phase flows is more complex than modelling sand erosion in single-phase flow. McLaury and Shirazi proposed a model for predicting erosion rates in multi-phase flows, based on the single-phase model by Shirazi. It consists of the same four steps as the single-phase flow model, but with a few modifications.

The stagnation length is calculated the same way as for single-phase, with Equation (3.19) for tees and Equation (3.20) for elbows.

In single-phase flow by Shirazi et al., the initial impact velocity is assumed to be equal to the flow velocity. In the multi-phase flow model by McLaury and Shirazi the sand is assumed to be located mainly in the liquid phase, thus the initial particle velocity is the same as the liquid velocity [McLaury and Shirazi, 2000].

The particle velocity is calculated in the same way as for single-phase flow, by Equation (3.28), but mixture density, ρ_m, and viscosity, μ_m are used instead of fluid density and viscosity. The mixture properties are found from the following equations:

$$\rho_m = \frac{V_{SG}}{V_{SL}+V_{SG}}\rho_G + \frac{V_{SL}}{V_{SL}+V_{SG}}\rho_L \tag{3.32}$$

$$\mu_m = \frac{V_{SG}}{V_{SL}+V_{SG}}\mu_G + \frac{V_{SL}}{V_{SL}+V_{SG}}\mu_L \tag{3.33}$$

where V_{SG} is superficial gas velocity, V_{SL} is superficial liquid velocity, ρ_G is the density of the gas, ρ_L is the density of the liquid, μ_G is the viscosity of the gas and μ_L is the viscosity of the liquid [McLaury and Shirazi, 2000].

The maximum erosion rate, ER, in a multi-phase flow is found from the following empirical equation:

$$ER = F_M F_S F_P F_{r/D} \frac{\dot{W}_p V_L^{1.73}}{(D/D_{ref})^2} \tag{3.34}$$

where F_M is a material factor, F_S is a particle shape factor, F_P is a penetration factor, $F_{r/D}$ is an elbow radius factor, $\dot{W}_p$ is the sand production rate, V_L is the characteristic impact velocity, D is the pipe diameter and D_{ref} is the reference pipe diameter (1 inch). For carbon steel materials, the material constant, F_M can be found from:

$$F_M = 1.95 \cdot 10^{-5}/B^{-0.59} \tag{3.35}$$

where B is the Brinell hardness factor [McLaury and Shirazi, 2000]. The particle shape factor, F_P and the particle shape factor, F_S can be found in Table A.2 and A.3 in Appendix A.2. The elbow radius factor $F_{r/D}$ can be calculated from the following equation:

$$F_{r/D} = \exp\left(-\left(0.1\frac{\rho_f^{0.4}\mu_f^{0.65}}{d_p^{0.3}} + 0.015\rho_f^{0.25} + 0.12\right)(\frac{r}{D} - 1.5)\right) \tag{3.36}$$

where r/D is the bend radius of curvature. In a standard elbow it is 1.5, and it is usually in the rage of 1.5 to 5 [McLaury and Shirazi, 2000].

The advantage of this model is that it takes many essential parameters into account, just like the model by Shirazi et al.. In addition, material factors, penetration factors and radius curvature factors are included. Multi-phase flow is to some degree taken into account by using mixture density and viscosity, and by assuming that the sand particles are located in the liquid flow. However, the various flow patterns that exist in multi-phase flows are not taken into account, and the fact that various flow patterns could make the particles behave differently is neglected. This simplification is one of the weaknesses of the McLaury and Shirazi model, but for many cases it could be a good simplification.

The model by McLaury and Shirazi is based on and validated against the experimental parameter presented in Table 3.5.

Table 3.5: The experimental values which the model by McLaury and Shirazi (2000) is based upon and validated against [McLaury and Shirazi, 2000]

Parameter	Symbol	Experimental range
Gas velocity	V_{SG}	3.5 - 107 m/s
Liquid velocity	V_{SL}	0.12 - 6.2 m/s
Particle diameter	d_p	150 - 350 μm
Pipe diameter	D	26.5 - 52.5 mm
Radius of curvature	r_c	1.5 - 5

Ad-hoc equations for the McLaury and Shirazi model

An alternative to using V_0 as the initial velocity in Equation 3.21 is to use the characteristic flow velocity. This gives the opportunity to take into account different multi-flow behaviours and patterns. The new equation for flow velocity profile is then:

$$V_f = V_{char}(1 - x/L) \tag{3.37}$$

The flow characteristic velocity, V_{char}, can be calculated from the following ad-hoc equations [Parsi et al., 2014]:

$$V_{char} = \lambda_L^n V_{SL} + (1 - \lambda_L)^n V_{SG} \tag{3.38}$$

where λ_L is:

$$\lambda_L = \left(\frac{V_{SL}}{V_{SL} + V_{SG}} \right)^{0.11} \tag{3.39}$$

and n is:

$$n = \left[1 - \exp\left(-0.25 \frac{V_{SG}}{V_{SL}} \right) \right] \tag{3.40}$$

Model by Mazumder et al. (2005)
Mazumder et al. developed a model based on the mechanistic model by Mclaury and Shirazi. For the same fluid velocities, different flow patterns can give different erosion rates. In this model, various flow patterns are taken into account by using the characteristic flow velocity to find a new particle initial velocity. The particle initial velocity is quite important in the calculation of erosion rates, as it has a big effect on the impact velocity. The erosion rate is determined by Equation (3.34) as before, but V_{char} is used instead of V_0 as in Equation (3.37), and V_{char} is calculated differently for each flow pattern [Parsi et al., 2014].

Different flow patterns in multi-phase flows occur because of interfacial forces between the phases. The most common flow patterns found in horizontal multi-phase flows are stratified flow, slug flow, annular flow and dispersed bubble flow. In vertical multi-phase flows the main flow patters are annular flow churn flow, slug flow and bubble flow [Parsi et al., 2014]. The different flow patterns are illustrated in Figure 3.12.

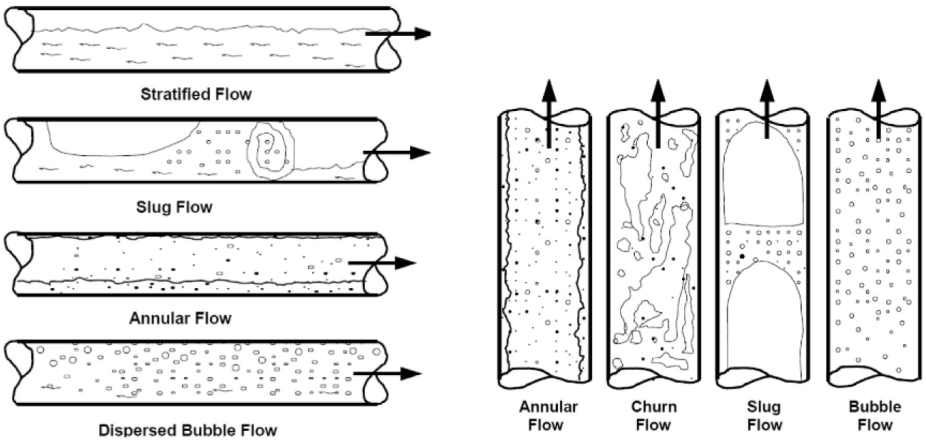

Figure 3.12: The main flow patterns in horizontal and vertical flows [Parsi et al., 2014]. **(a)** Main flow patterns in horizontal pipes: stratified flow, slug flow, annular flow and dispersed bubble flow. **(b)** Main flow patterns in vertical flows: annular flow, churn flow, slug flow and bubble flow.

Slug flow
Slug flow is a multi-phase flow with an alternation of liquid slugs and gas pockets. It occurs in a wide range of liquid and gas rates. In the model by Mazumder et al. it is assumed that the sand particles are evenly distributed in the liquid phase and that the mass fraction of sand in the liquid slugs equals the mass fraction of liquid in liquid slugs. Sand erosion in the liquid film i neglected. The characteristic fluid velocity is then:

$$V_{char} = H_{LLS} \cdot V_{LLS} \tag{3.41}$$

where H_{LLS} is the liquid holdup in the slug body and V_{LLS} is the velocity of the slug body [Mazumder et al., 2004]. The liquid holdup can be found from a correlation by Gomez:

$$H_{LLS} = \exp\left(-(0.45\theta + 2.48 \times 10^{-6} \cdot \frac{\rho_L V_m D}{\mu_L})\right) \tag{3.42}$$

where θ is the inclination angle between 0 and 90 degrees and $V_m = V_{SG} + V_{SL}$ [Gomez et al., 2000].

The liquid velocity of the slug body can be found from the following equation

$$V_{LLS} = \frac{V_m - V_{GLS}(1 - H_{LLS})}{H_{LLS}} \tag{3.43}$$

where V_{GLS} is the velocity of the gas in the liquid slugs [Mazumder et al., 2004].

Bubble flow
Bubble flow occurs at low gas velocities and high liquid velocities. The flow has a continuous liquid phase with evenly distributed gas bubbles [Parsi et al., 2014]. In the model by Mazumder et al. it is assumed that the sand is evenly distributed in the liquid phase and that the sand particle initial velocity is the same as the mixture velocity:

$$V_{char} = V_m = V_{SL} + V_{SG} \tag{3.44}$$

where V_{SL} is the superficial liquid velocity and V_{SG} is the superficial gas velocity [Mazumder et al., 2004].

Mazumder's model to predict erosion rates in slug and bubble flows are validated against the experimental values presented in Table 3.6. The model appears to be good in the range of these parameters.

Table 3.6: The experimental values in which the model for slug flow and bubble flow by Mazumder (2005) is based upon and validated against [Mazumder et al., 2004].

Parameter	Symbol	Experimental range
Gas velocity	V_{SG}	3.5 - 15 m/s
Liquid velocity	V_{SL}	0.2 - 6.2 m/s
Pipe diameter	D	26.5 - 49 mm
Radius of curvature	r_c	5
Characteristic velocity	V_{char}	5.2 - 14.3 m/s
Particle diameter	d_p	150 - 250 μm

Annular flow
Annular flow is characterized by a gas phase distributed as entrained bubbles in a continuous liquid phase. A thin liquid film is surrounding the pipe wall. Annular flow occurs when the gas velocity is high and the liquid velocity is low [Parsi et al., 2014].

The initial particle velocities in the liquid and gas flows can be found from the following equations:

$$V_{0L} = V_{film} \tag{3.45}$$

$$V_{0G} = V_{droplet} \tag{3.46}$$

where V_{film} is the liquid film velocity and $V_{droplet}$ is the liquid droplet velocity. The liquid film velocity can be found from the following equation:

$$V_{film} = V_{SL}\frac{(1-E)D^2}{4\delta_{film}(D-\delta_{film})} \tag{3.47}$$

where D is the pipe diameter, δ_{film} is the thickness of the liquid film and E is the liquid droplet entrainment fraction. E can be found from the following equation:

$$E = \tanh(7.25 \cdot 10^{-7}\mathrm{We}^{1.25}\mathrm{Re}_L^{0.25}) \tag{3.48}$$

where We is a modified Weber number and Re_L is the liquid Reynolds number, which can be found from:

$$\mathrm{We} = \frac{\rho_G V_{SG}^2 D}{\sigma}\left(\frac{\rho_L - \rho_G}{\rho_G}\right)^{1/3} \tag{3.49}$$

$$\mathrm{Re}_L = \frac{\rho_L V_{SL} D}{\mu_L} \tag{3.50}$$

where σ is the surface tension [N/m]. The droplet velocity can be found from the following equation:

$$V_{droplet} = 0.8 V_{G_{core}} \tag{3.51}$$

where $V_{G_{core}}$ is the gas core velocity:

$$V_{G_{core}} = V_{SG}\left(\frac{D}{D-2\delta_{film}}\right)^2 \tag{3.52}$$

Mazumder's erosion model for annular flow is validated against the experimental parameters in Table 3.7.

Table 3.7: The experimental values in which the model by Mazumder (2005) for anuular flow is based upon and validated against [Mazumder et al., 2004].

Parameter	Symbol	Experimental range
Gas velocity	V_{SG}	14 - 107 m/s
Liquid velocity	V_{SL}	0.1 - 5.8 m/s
Pipe diameter	D	26.5 - 52.5 mm
Radius of curvature	r_c	1.5 - 5
Characteristic velocity	V_{char}	6.8 - 107 m/s
Particle diameter	d_p	150 - 350 μm
Liquid film thickness	δ_{liquid}	134 - 2144 μm

The characteristic flow velocity can then be found from the following equation [Mazumder et al., 2004]:

$$V_{char} = (1 - E)V_{film} + E \cdot V_{droplet} \tag{3.53}$$

Churn flow
Churn flow is characterized by liquid lumps moving up and down. There are no clear phase boundaries, and the flow appears to be a mix of annular flow and slug flow. Churn flow occurs when the gas rates are high. There are not many studies on churn flow because of the complexity of this flow. Mazumder suggests that the characteristic fluid velocity equals the mixture velocity, but because of the lack in data, this is yet to be properly validated [Mazumder et al., 2004].

Model by Chen et al. (2006)
The model by Chen et al. also takes multi-phase flow patterns into account, but unlike the model by Mazumder it is not based on the model by Mclaury and Shirazi. The first step of the Chen et al. model is to simplify the multi-phase flow to a representative single-phase. Important flow parameters are considered, which could be different for each flow pattern. The effective sand mass ratio, defined by the mass of sand in the representative single-phase flow divided by the total mass of sand in the gas/liquid/sand flow, is also calculated. The second step is to apply a single-phase CFD-based model to predict the erosion in the flow. This is weighted by the sand mass ratio to get the estimated erosion rate [Chen et al., 2005].

Slug flow
It is assumed that the sand particles are located in the liquid phase only, and erosion in the liquid film is neglected. It is therefore possible to simplify the system to a single-phase flow system with the mixture properties of the slug unit or the slug body. For the slug body the mixture properties can be calculated from the following equations:

$$\rho_m = (1 - H_{LS})\rho_G + H_{LS}\rho_L \tag{3.54}$$

$$\mu_m = (1 - H_{LS})\mu_G + H_{LS}\mu_L \tag{3.55}$$

where H_{LS} is the liquid holdup for the slug body. For the slug unit, the mixture viscosity is calculated from Equation (3.33) and the mixture density is calculated from:

$$\rho_m = (1 - H_L)\rho_G + H_L\rho_L \tag{3.56}$$

where H_L is the in situ liquid holdup. The liquid mass ratio is calculated by:

$$\dot{m} = \frac{l_S H_{LS} V_m}{l_S H_{LS} V_m + l_F H_{LF} V_F} \tag{3.57}$$

where l_S is the slug length,H_{LS} is the slug liquid holdup, l_F is the liquid film length, H_{LF} is the liquid film holdup and V_m is the mixture velocity: $V_M = V_{SG} + V_{SL}$.

l_S, H_{LS}, H_{LF} and V_F is found from Zhang's model [Zhang et al., 2003]:

$$l_S = (32.0\cos^2\theta + 16.0\sin^2\theta) \cdot D \tag{3.58}$$

$$H_{LS} = \frac{1}{1 + (\frac{V_S}{8.66})^{1.39}} \tag{3.59}$$

$$H_{LF} = \frac{(H_{LS}(V_T - V_S) + V_{SL})(V_{SG} + V_{SL}E) - V_T V_{SL} E}{V_T V_{SG}} \tag{3.60}$$

$$V_F = \frac{V_{SL}(1-E)}{H_{LF}} \tag{3.61}$$

where θ is the inclination angle, D is the pipe diameter, V_S is the velocity of the slugs, V_T is the translational velocity of liquid slugs, V_{SL} is the superficial liquid velocity, V_{SG} is the superficial gas velocity and E is the liquid entrainment fraction in the gas core. The entrainment fraction can be calculated from Equation (3.48) and the translational velocity can be found from:

$$V_T = C_S V_S + V_D \tag{3.62}$$

where C_S is a coefficient (1.2 for turbulent flow and 2 for laminar flow), V_S is the velocity of the slugs and V_D is the drift velocity. V_D can be found from:

$$V_D = 0.54\sqrt{g \cdot D}\cos(\theta) + 0.35\sqrt{g \cdot D}\sin\theta \tag{3.63}$$

where g is the gravity acceleration [Zhang et al., 2003, Chen et al., 2005].

In the model by Chen et al., the erosion rate is underestimated when the slug body mixture properties are used. Using the mixture properties of the slug unit gives a better estimation, most likely because it gives a more physical representation in elbow geometries [Chen et al., 2005]. The experimental data in which the model is validated against is presented in Table 3.8

Table 3.8: The experimental values in which the model by Chen (2005) for slug flow is validated against [Chen et al., 2005].

Parameter	Symbol	Experimental range
Gas velocity	V_{SG}	8 - 34 m/s
Liquid velocity	V_{SL}	0.2 - 3.1 m/s
Mixture density	ρ_m	26.62 - 136.19 kg/m^3
Pipe diameter	D	26.5 - 49 mm
Radius of curvature	r_c	1.5 - 5
Particle diameter	d_p	150 - 250 μm

Bubble flow
It is assumed that the flow is homogeneous, and the multi-phase flow is simplified to a single-phase where the fluid has the mixture fluid properties of the two phases. Equation (3.56) is used to calculate the mixture density, Equation (3.33) is used to calculate the mixture viscosity and the mixture velocity is found from $V_m = V_{SG} + V_{SL}$. The effective sand mass ratio equals 1 because the single-phase flow contains the same amount of sand as the bubbly flow. This model was found to be very good when compared to experimental results [Chen et al., 2005]. The experimental in which the model is validated against is presented in Table 3.9

Table 3.9: The experimental values in which the model by Chen (2005) for bubble flow is validated against [Chen et al., 2005].

Parameter	Symbol	Experimental range
Gas velocity	V_{SG}	3.5 - 10 m/s
Liquid velocity	V_{SL}	4 - 6.2 m/s
Mixture density	ρ_m	334.87 - 534.41 kg/m^3
Pipe diameter	D	26.5 - 49 mm
Radius of curvature	r_c	5
Particle diameter	d_p	150 - 250 μm

Annular flow
It is assumed that the erosion in mainly caused by the sand in the gas core. The gas/liquid/sand flow in the gas core is considered as a single-phase flow, and the erosion is predicted in the gas core. In addition, the liquid film is considered, as it gives a cushioning effect on the particle impact. The effective sand mass ratio is assumed to be equal to the liquid droplet entrainment

fraction, which can be calculated from Equation (3.48). The mixture density can be found from Equation (3.56) and the mixture viscosity found from Equation (3.33). The mixture velocity can be found from:

$$V_m = V_{SG} + V_{DSG} \tag{3.64}$$

where V_{SG} is the superficial gas velocity and V_{DSG} is the droplet superficial velocity in the gas core. It was found that the model gave better predictions when the liquid film cushioning effect was added, and that the model gave reasonable results [Chen et al., 2005]. The model was validated against the experimental values presented in Table 3.10.

Table 3.10: The experimental values in which the model by Chen (2005) for annular flow is validated against [Chen et al., 2005].

Parameter	Symbol	Experimental range
Gas velocity	V_{SG}	30 - 52 m/s
Liquid velocity	V_{SL}	0.5 - 1.5 m/s
Mixture density	ρ_m	21.5 - 42.5 m/s
Pipe diameter	D	26.5 - 49 mm
Radius of curvature	r_c	5
Particle diameter	d_p	150 - 250 μm

DNV-GL Reccomended practice (2015)
DNV-GL has developed a quite extensive model for estimating sand erosion rates in both straight pipes, elbows, tees, reducers and welded joints. The model is based on experimental data and CFD-results, and can be found in their guideline "Managing sand production and erosion" [DNV-GL, 2015b]. The input parameters in this model are limited to the range that is presented in Table 3.11.

Table 3.11: The limited range of the erosion model by DNV-GL [DNV-GL, 2015b].

Parameter	Symbol	Limited range
Particle diameter	d_p	0.02 - 5 mm
Particle density	rho_p	2000 - 3000 kg/m^3
Pipe diameter	D	0.01 - 1 m
Radius of bend		0.5 - 50
Pipe material density	ρ_t	1000 - 16 000 kg/m^3
Liquid velocity	V_{SL}	0 - 50 m/s
Gas velocity	V_{SG}	0 - 200 m/s
Liquid density	ρ_L	200 - 1500 kg/m^3
Gas density	ρ_G	1 - 600 kg/m^3
Liquid viscosity	μ_L	10^{-5} - 10^{-2} kg/ms
Gas viscosity	μ_G	10^{-6} - 10^{-4} kg/ms
Particle concentration		0 - 500 ppmV

Straight pipes
Erosion rates in straight pipes are usually not high, especially compared to other parts of the piping system. This is mostly due to the low impact angle. The erosion rate in mm/year can be found from:

$$ER = 2.5 \cdot 10^{-5} \cdot V_p^{2.6} \cdot D^{-2} \cdot m_p \tag{3.65}$$

where V_p is the particle velocity in m/s, D is the diameter of the pipe in m and m_p is the mass rate of sand in kg/s [DNV-GL, 2015b].

Elbows
The maximum erosion rate ER in the choke valve [mm/year] can be found from the following equation:

$$ER = \frac{K \cdot F(\alpha) \cdot V_p^n}{\rho_t \cdot A_t} \cdot G \cdot C_1 \cdot GF \cdot m_p \cdot C_{unit} \tag{3.66}$$

where K, n, C_1, GF and C_{unit} are various constants. $F(\alpha)$ is the ductility of the material, α is the characteristic impact angle in radians, V_p is the particle impact velocity in m/s, ρ_t is the density of the target material kg/m^3, A_t is the area exposed to erosion in m^2 and m_p is the mass rate of sand in kg/s [DNV-GL, 2015b].

K is a material erosion constant and n is a velocity constant. Values for these constants can be found in Table A.4. C_1 is a model geometry factor which

in the case of an elbow geometry is set to 2.5. GF is a geometry factor that depends on the upstream pipe configuration. A complete overview of which geometry factor should be chosen at specific cases can be found on page 25 in "Managing sand production and erosion" by DNV-GL. In the case of unknown piping complexity, the geometry factor is set to 2. C_{unit} is the unit conversion factor that convert the erosion rate unit from m/s to mm/year, and equals $3.15 \cdot 10^{10}$ [DNV-GL, 2015b].

The ductility of the target material is characterised by the function $F(\alpha)$. An overview of which materials are considered brittle or ductile is shown in table A.4. $F(\alpha)$ for ductile materials can be found from:

$$F(\alpha)_{ductile} = 0.6 \cdot [\sin(\alpha) + 7.2(\sin(\alpha) - \sin^2(\alpha))]^{0.6} \cdot [1 - \exp(-20\alpha)] \quad (3.67)$$

where α is the characteristic impact angle. $F(\alpha)$ for brittle materials can be found from:

$$F(\alpha)_{brittle} = \frac{2\alpha}{\pi} \quad (3.68)$$

In both cases the value of $F(\alpha)$ is between 0 and 1 [DNV-GL, 2015b].

The characteristic impact angle, α, can be found from the following equation:

$$\alpha = \arctan(\frac{1}{\sqrt{2R}}) \quad (3.69)$$

where R is the radius of curvature [DNV-GL, 2015b].

The area exposed to erosion, A_t, is:

$$A_t = \frac{\pi D^2}{4 \cdot \sin(\alpha)} \quad (3.70)$$

where D is the pipe diameter and α is the impact angle [DNV-GL, 2015b].

G is the particle size correction function and can be found from:

$$G = \begin{cases} \gamma/\gamma_c, & \text{if } \gamma < \gamma_c \\ 1, & \text{if } \gamma \geq \gamma_c \end{cases} \quad (3.71)$$

γ can be determined from the following equations:

$$\gamma = \frac{d_p}{D} \quad (3.72)$$

where d_p is the particle diameter and D is the pipe diameter. γ_c can be found from:

$$\gamma_c = \begin{cases} \frac{1}{\beta \cdot [1.88 \cdot \ln(A) - 6.04]}, & \text{if } \gamma_c < 0.1 \\ 0.1, & \text{if } \gamma_c > 0.1 \vee \gamma_c \leq 0 \end{cases} \tag{3.73}$$

where the dimensionless parameters A and β can be determined from:

$$A = \frac{\rho_m^2 \cdot \tan(\alpha) \cdot V_p \cdot D}{\rho_p \cdot \mu_m} \tag{3.74}$$

$$\beta = \frac{\rho_p}{\rho_m} \tag{3.75}$$

where ρ_m is the mixture density, α is the impact angle, V_p is the particle velocity, D is the pipe diameter, ρ_p is the density of the particle and μ_m is the mixture viscosity [DNV-GL, 2015b].

Tees
The maximum erosion rate in a tee can be estimated from the following equation:

$$ER = \frac{m_p \cdot K \cdot V_p^n}{\rho_t \cdot A_t} \cdot G \cdot C_1 \cdot GF \cdot m_p \cdot C_{unit} \tag{3.76}$$

In this case K, n and GF are found in the same way as for elbows. ρ_t is the density of the target material, m_p is the mass rate of sand, V_p is the particle velocity and C_{unit} is $3.15 \cdot 10^{10}$. The area exposed to erosion can be calculated from the following equation:

$$A_t = \frac{\pi D^2}{4} \tag{3.77}$$

where D is the diameter of the pipe. To find G and C_1 the following dimensionless parameters must be calculated:

$$\gamma = \frac{d_p}{D} \tag{3.78}$$

$$\beta = \frac{\rho_p}{\rho_m} \tag{3.79}$$

$$\mathrm{Re_D} = \frac{V_m \cdot D}{\nu_m} \tag{3.80}$$

where d_p is the particle diameter, D is the pipe diameter, ρ_p is the density of the particle, ρ_m is the mixture fluid density, V_m is the mixture fluid velocity and ν is the kinematic viscosity of the mixture fluid [DNV-GL, 2015b].

For cases where $\beta < 40$, the following parameters are set:

$$C_1 = \frac{3}{\beta^{0.3}} \tag{3.81}$$

$$\gamma_c = \frac{0.14}{\beta} \tag{3.82}$$

$$c = \begin{cases} \frac{19}{\ln(\mathrm{Re_D})}, & \text{if } \gamma < \gamma_c \\ 0, & \text{if } \gamma \geq \gamma_c \end{cases} \tag{3.83}$$

In cases where $\beta \geq 40$ the following parameters are set:

$$C_1 = 1.0 \tag{3.84}$$

$$b = \left[\ln\left(\frac{\mathrm{Re_D}}{10000} + 1\right) + 1\right]^{-0.6} - 1.2 \tag{3.85}$$

$$\gamma_c = 0.0035\left(\frac{\beta}{40}\right)^b \tag{3.86}$$

$$c = \begin{cases} \frac{19}{\ln(\mathrm{Re_D})}, & \text{if } \gamma < \gamma_c \\ -0.3 \cdot (1 - 1.01^{40-\beta}), & \text{if } \gamma \geq \gamma_c \end{cases} \tag{3.87}$$

The particle size correction function can then be found from the following equation [DNV-GL, 2015b]:

$$G = \left(\frac{\gamma}{\gamma_c}\right)^c \tag{3.88}$$

Reducers
Reducers can be prone to sand erosion because of the flow acceleration and the change in flow direction. An illustration of a reducer with some important parameters are shown in Figure 3.13.

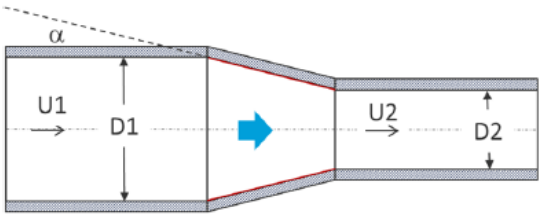

Figure 3.13: An illustration of a reducer with some of the important parameters. This illustration is taken from DNV-GL's "Managing sand production and erosion" [DNV-GL, 2015b].

The maximum erosion rate in a reducer is calculated from the following equation:

$$ER = \frac{K \cdot F(\alpha) \cdot V_p^n}{\rho_t \cdot A_t} \cdot A_{ratio} \cdot C_2 \cdot GF \cdot m_p \cdot C_{unit} \tag{3.89}$$

In this case K, $F(\alpha)$, n and GF are found in the same way as for elbows. ρ_t is the density of the target material, m_p is the mass rate of sand and C_{unit} is $3.15 \cdot 10^{10}$. The area exposed to erosion, A_t, can be calculated from the following equation:

$$A_t = \frac{\pi}{4 \cdot \sin(\alpha)} \cdot (D_1^2 - D_2^2) \tag{3.90}$$

where α is the impact angle and D_1 and D_2 are the diameter of the pipe, before and after the pipe reduction, respectively [DNV-GL, 2015b].

The particle velocity can be found from the following equation:

$$V_p = V_{m,2} = V_{m_1} \cdot \left(\frac{D_1}{D_2}\right)^2 \tag{3.91}$$

where $V_{m,1}$ is the mixture velocity at cross section 1 (before the impact) [DNV-GL, 2015b].

The ratio between the area exposed to particle impacts and the area before the pipe reduction, A_{ratio}, can be found from [DNV-GL, 2015b]:

$$A_{ratio} = 1 - \left(\frac{D_2}{D_1}\right)^2 \tag{3.92}$$

The particle size and fluid density correction function is calculated from the following equation:

$$C_2 = \begin{cases} \frac{10^6 \cdot d_p}{30 \cdot (\rho_m)^{1/2}}, & \text{if } \frac{10^6 \cdot d_p}{30 \cdot (\rho_m)^{1/2}} < 1 \\ 1, & \text{if } \frac{10^6 \cdot d_p}{30 \cdot (\rho_m)^{1/2}} \geq 1 \end{cases} \tag{3.93}$$

where d_p is the diameter of the particle and ρ_m is the mixture fluid velocity [DNV-GL, 2015b].

Welded joints
The change in the geometry of the weld as it is eroded is not taken into account in this model. The maximum erosion rate in a welded joint has to be determined for both the upstream and downstream side of the weld. This is illustrated in Figure 3.14 as well as some of the key parameters.

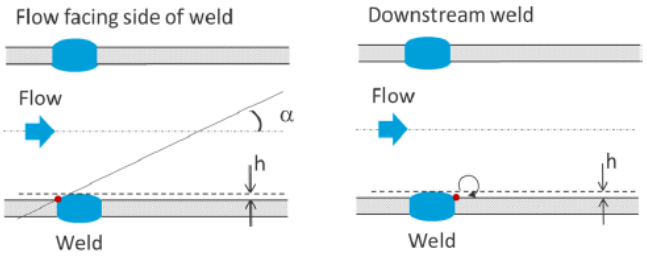

Figure 3.14: Sand erosion modelling in welded joints upstream and downstream of the weld. α is the angle between the weld and direction of the flow and h is the height of the weld. This illustration is taken from DNV-GL's "Managing sand production and erosion" [DNV-GL, 2015b].

The upstream erosion rate can be found from the following equation:

$$ER = K \cdot F(\alpha) \cdot V_p^n \cdot \frac{\sin(\alpha)}{\rho_t \cdot A_{pipe}} \cdot C_2 \cdot C_{unit} \cdot m_p \tag{3.94}$$

where K, $F(\alpha)$, V_p, n, ρ_t, C_{unit} and m_p are the same as for elbows. A_{pipe} is the cross sectional area of the pipe. The impact angle α is usually estimated. or if unknown chosen to be 60°. The particle size and fluid density correction function C_2 can be found from Equation (3.93). The downstream erosion rate can be estimated from the following equation:

$$ER = 3.3 \cdot 10^{-2} \cdot (7.5 \cdot 10^{-4} + h) \cdot V_p^{2.6} \cdot D^{-2} \cdot m_p \tag{3.95}$$

where h is the height of the weld, V_p is the particle velocity, D is the diameter of the pipe and m_p is the mass rate of sand [DNV-GL, 2015b].

Computational fluid dynamics - based models

Computational fluid dynamics (CFD) - based erosion modelling can be a very powerful tool to assess erosion problems, and many researchers use CFD to simulate sand erosion. CFD-modelling generally consists of three steps:

1. Flow modelling
2. Particle tracking

3. Erosion calculation

Each step depends on the results obtained in the first one, which mean that any faulty or non-physical results will affect the final result. The three steps are illustrated in Figure 3.15 [Parsi et al., 2014].

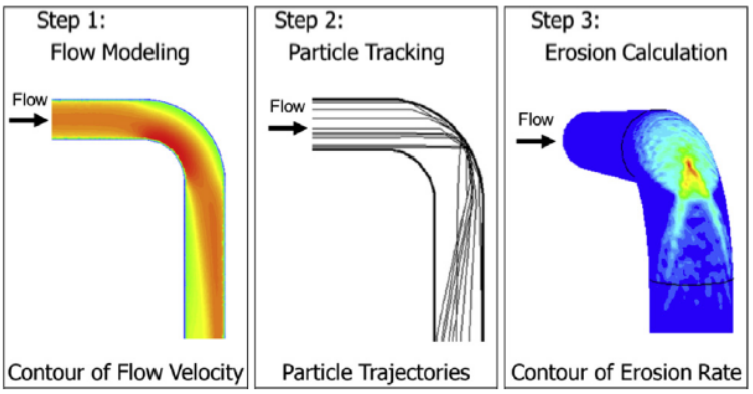

Figure 3.15: The three steps of CFD-based erosion modelling: flow modelling, particle tracking and erosion calculation [Parsi et al., 2014].

The flow modelling is usually performed by CFD software such as CFX, STAR-CCM+ and FLUENT. Navier-Stokes equations are solves to find field data such as pressure, velocity and kinetic energy in turbulent flow. This calculation can be computationally expensive, and often time-averaged forms of the Navier-Stokes equations are used instead. As a consequence, turbulent fluctuations are small-scaled. Reynolds stresses are therefore introduced, and the need for closure equations arises. The closure equations are found from various turbulence models, and great care should be put into selecting an appropriate turbulence model. Once a proper turbulence model is found, a CFD mesh sensitivity analysis should be performed to make sure that the flow field is not depending on the mesh and that the calculations are accurate [Parsi et al., 2014].

When performing the particle tracking in the second step, a Lagrangian or Eulerian approach is used to simulate the motion of the particle. In the Eulerian approach, the particles are considered to be a continuous phase. The following transportation equation is used:

$$\frac{\delta \rho C}{\delta t} + \frac{\delta}{\delta x_i}(\rho \overline{u_i} C - \Gamma \frac{\delta C}{\delta x_i}) = S_c \tag{3.96}$$

where ρ is the density of the fluid, C is the particle concentration, t is the time, x_i with $i = 1, 2, 3$ are the coordinates, $\overline{u_i}$ is the fluid velocity in three

directions, Γ is the effective particle diffusivity and S_c is the particle source term. In the Eulerian method, many iterations are performed on this equation to obtain a converged solution [Zhang and Chen, 2007].

In the Lagrangian approach, particles are considered to be a dispersed phase in the continuous fluid phase. The particle equation of motion is used to track each particle:

$$\frac{dV_p}{dt} = F_D + F_V + F_P + F_G \tag{3.97}$$

where F_D is the drag force, F_V is the virtual mass force, F_P is the pressure gradient force and F_G is the gravity and buoyancy force. The Saddman lift force can also be included in this equation [Parsi et al., 2014]. The Lagrangian method tracks the particle in each time step and does not need to iterate as long as the particles are not coupled with the fluid phase. However, a large number of particle trajectories are calculated, and this may have to be repeated many times to get a stable solution [Zhang and Chen, 2007].

The Lagrangian approach is usually preferred over the Eulerian method, as the Eulerian method is not good for predicting particle behaviour close to the wall. This is problematic when modelling sand erosion, as what is modelled is a particle impacting a wall. However, the Eulerian method is sometimes used when the concentration of particles in the fluid is high, as the Lagrangian method then becomes computationally expensive [Parsi et al., 2014].

Whenever a particle impacts a wall, some of its energy is lost in the impact. Restitution coefficients are used to account for this loss. The restitution coefficient for impacts in a normal direction, e_n can be found from the following equation:

$$e_n = \frac{V_{pn2}}{V_{pn1}} \tag{3.98}$$

where V_{pn2} is the particle velocity after the impact and V_{pn1} is the particle velocity before the impact. The restitution coefficient for impact in a tangential direction can be found in a similar manner:

$$e_t = \frac{V_{pt2}}{V_{pt1}} \tag{3.99}$$

where V_{pt2} is the velocity of the particle after the impact and V_{pt1} the velocity of the particle before the impact [Parsi et al., 2014].

The third step of CFD-based erosion models is to use the information obtained so far in an erosion equation to predict the erosion damage by each

particle impact. At last, all of the impacts is summarized to find the total erosion rate [Parsi et al., 2014].

Model by Sundararajan and Shewmon (1982)
Sundararajan and Shewmon developed a theoretical model for erosion of metals. A derivation of this model can be found in the article by Sundararajan and Shewmon [Sundararajan and Shewmon, 1982].

A simplified form of their model is given as:

$$\epsilon_s \approx \frac{6.5 \cdot 10^{-3} V_p^{2.5} \rho_p^{0.25}}{C_p T_m^{0.75} H_t^{0.25}} \tag{3.100}$$

where V_p is the particle velocity in m/s , ρ_p is the particle density in kg/m^3, C_p is the target heat capacity in J/(kg K), T_m is the target melting point in K and H_t is the hardness of target in Mpa. ϵ_s is a dimensionless parameter that expresses the mass of material removed per mass of erodent [Sundararajan and Shewmon, 1982].

3.2.4 Modelling sand erosion in choke valves

Choke valves can be very exposed to sand erosion and may have to be replaced every 3-24 months because of of it. There have even been cases when the critical components of a choke valve have been destroyed within a few hours because of sand. Replacing choke valves are costly and unwanted. Most models for sand erosion in choke valves are empirical, as the complex geometry of the valve makes it difficult and costly to do mechanistic or CFD-based calculations. Today, the problem of sand erosion in choke valves is dealt with by selecting erosion resistant materials for the valve components and choosing valve geometries less prone to erosion [Haugen et al., 1995].

DNV-GL Recommended practice (2015)
DNV-GL developed a model to estimate the erosion in a choke valve based on the erosion model for an elbow (Equation (3.66) to Equation (3.75)). In figure 3.16 a generic choke gallery is shown along with the dimension parameters needed to estimate the rate of erosion.

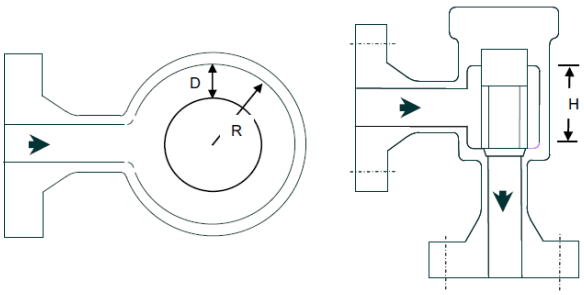

Figure 3.16: A generic choke gallery and the dimensions needed to estimate the erosion rate ER. R is the radius of curvature, D is the gap between the choke body and cage and H is the height of the gallery [DNV-GL, 2015b].

A few changes are made to the choke model: The radius of curvature R is now the radius of the choke gallery, H is the height of the gallery and D is the gap between the cage and the choke body (as seen in Figure 3.16). The particle impact velocity is in this model found from:

$$V_p = \frac{3}{4} \cdot \frac{Q}{A_g} \tag{3.101}$$

where Q is the actual flow rate in m^3/s and A_g is the effective gallery area. A_g can be found from the following equation:

$$A_g = 2 \cdot H \cdot D \tag{3.102}$$

and C_1 is set to be 1.25 [DNV-GL, 2015b].

This empirical model by DNV-GL is limited to a generic choke. The erosion rates have been compared to CFD-simulations and some full scale experiments. Based on this, it has been concluded that the model should not be considered more accurate than a factor of $\pm$ 3 for the predicted erosion [DNV-GL, 2015b].

Model by Haugen et al. (1995)
In the model by Haugen et al., the following generic sand erosion equation is used to calculate the erosion rate:

$$E = M_p \cdot K \cdot F(\alpha) \cdot V_p^n \tag{3.103}$$

where M_p is the mass of sand hitting the target material, K and n are material dependent constant, $F(\alpha)$ is a function describing the effect of the impact angle α on the material. This is an empirical equation not specifically designed for choke valves, but Haugen et al. performed experiments to find

proper parameters K, $F(\alpha)$ and n, so that the equation would be valid for choke valves as well [Haugen et al., 1995].

Based on experiments, the function $F(\alpha)$ was determined to be:

$$F(\alpha) = \Sigma_{i=1}^{8}(-1)^{(i+1)}A_i\left(\frac{\alpha\pi}{180}\right) \tag{3.104}$$

where the values of A_i is given in Table A.5 in Appendix A.4. Values of K and n can be found in Table A.4 in Appendix A.3 [Haugen et al., 1995].

The velocity of the particles was estimated using CFD-calculations. Comparing modelling erosion rates with experimental erosion rates proved that this model can be considered valid within the range of the experiment. It was also concluded that the model could be extrapolated for design purposes [Haugen et al., 1995]. The experimental values in which the model is validated against are shown in Table 3.12.

Table 3.12: The range of experimental parameters in the experiments performed by Haugen et al. used to determine $F(\alpha)$ and the parameters A_i in Equation 3.104 [Haugen et al., 1995].

Parameter	Experimental range
Particle diameter	200-250 um
Pipe length	2 m
Pipe diameter	6 mm
Air velocity	22 - 320 m/s
Impact angle	22.5 - 90.0°

3.3 Corrosion

Corrosion is one of the most common failure mechanisms in the oil and gas industry. World-wide it is assumed that the annual corrosion cost of the oil and gas industry exceeds 60 billion USD. Reducing the costs related to corrosion is therefore very important. Corrosion is common in almost all subsea equipment, such as pipelines, wellheads, valves, separators, compressors and pumps [Papavinasam, 2014].

Corrosion control strategies depend on the type of corrosion, but some common strategies are proper material selection, applying corrosion-resistant

coatings, adding lubricants, adjusting the temperature, and adding corrosion inhibitors. Which corrosion control strategy is used depends on the type of corrosion [Papavinasam, 2014]. Figure 3.17 shows two pipes that have been damaged by corrosion.

(a) **(b)**

Figure 3.17: Corrosion damage in pipes. **(a)** Corrosion inside a pipe [Huguenot Laboratories, nd] . **(b)** Corrosion damage in a pipe has lead to a hole in the pipe [Colorado Geological Survey, nd].

Corrosion is a huge field and many books have been written about this topic alone. It is therefore impossible to cover everything in this thesis, and this section remains a brief overview of corrosion. This section will be focused on the mechanism of corrosion, important corrosion parameters and finally present a selection of models used to calculate corrosion rate in subsea equipment.

3.3.1 The chemistry of corrosion

Corrosion is an electrochemical reaction that takes place in aqueous solutions. The four essential elements for corrosion are: an anode, a catode, an electrolyte and a conductor. The anode is where the oxidation reaction occur. This reaction is the corrosion process. The metal loses electrons, making metal ions leave the surface and enter the electrolyte. A general anodic reaction is as following:

$$\mathrm{M} \longrightarrow \mathrm{M}^{n+} + \mathrm{ne}^{-} \tag{3.105}$$

The electrons remain on the anode while the ions travel from the metal through the electrolyte to the cathode. Electrolytes contain negatively charged anions and positively charges cations. The anions will move towards the positive anode while the cations will move towards the negative cathode.

The conductor transports the electrons from the anode to the cathode. At the cathode there is a reduction reaction. Metallic ions from the electrolyte reacts with electrons transported to the cathode, causing a deposition of metal on the cathode. A general cathodic reaction is:

$$M^{n+} + ne^- \longrightarrow M \tag{3.106}$$

An illustration of how corrosion on a steel surface works can be found in Figure 3.18. Both the anode and cathode exist on the same piece of metal, which also functions as a conductor. The electrolyte could be seawater or fluid from production. Steel consists of iron (Fe) that can readily be oxidized. Fe^{2+} ions react with O_2, CO_2 and H_2O in the electrolyte. Rust (Fe_2O_3), iron carbonate (Fe_2CO_3) and iron sulfides (FeS_x) are formed on the material surface. Hydrogen gas is formed at the cathode [Brondel et al., 1994].

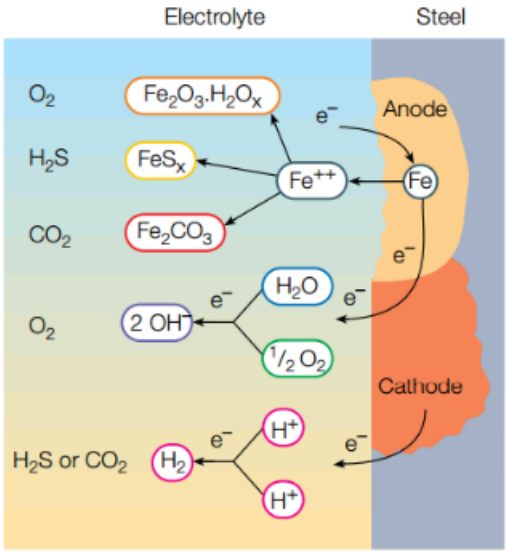

Figure 3.18: Corrosion mechanism on a metal surface: Rust (Fe_2O_3), iron carbonate (Fe_2CO_3) and iron sulfides (FeS_x) are formed on the material surface from oxidation reactions. Hydrogen gas is formed on the cathode [Brondel et al., 1994].

3.3.2 Different types of corrosion

There are many types of corrosion. Not all types are described in this section, but a complete list can be found in Table A.6 in Appendix A.5.

General corrosion

General corrosion occurs in the manner described in Section 3.3.1 and illustrated in Figure 3.18. The cathode and anode are located on the same piece

of metal. Uniform corrosion is often assumed, even though it is generally not the case. When the surface is fully covered by corrosion products, no more corrosion takes place. General corrosion is usually avoided by proper material selection and corrosion inhibitors [Papavinasam, 2014].

Galvanic corrosion
Galvanic corrosion is a type of corrosion that happens when dissimilar alloys and metals are in contact with each other and a conductive solution. One material will then be less prone to corrosion than the other. This material becomes the anode and the corrosion increases at this site. The less corrosive material becomes the cathode and the corrosion decreases. In other words, the corrosion is higher for metals and alloys because they are in contact with other metals and alloys. This type of corrosion is prevented by selecting materials close to each other in the galvanic series to lower the potential between them [Papavinasam, 2014]

Pitting corrosion
If the surface area of the anode and cathode is different, localized corrosion occurs. The corrosion will be greater in some of the surface areas. If the corrosion takes place in a small area, small holes are formed in the surface of the material. This is called pitting erosion. Corrosion inhibitors and proper material selection are control strategies to minimize pitting corrosion [Papavinasam, 2014].

Crevice corrosion
Crevice corrosion orrosion may happen in tiny cracks and crevices in the production equipment. The crevice must be shielded so that there is stagnant solution, but not so much that liquid is prevented from entering. Crevice corrosion is usually controlled in the design phase by avoiding crevices in equipment [Papavinasam, 2014].

Fretting corrosion
Fretting corrosion is also known as false Brinelling, chafing, wear oxidation and friction oxidation. It is a type of corrosive wear, as described in Section 3.1.4. Fretting corrosion occurs in contact areas between materials under load because of vibration and slip. Fretting corrosion is usually controlled by applying lubricants to reduce the friction between the surfaces [Papavinasam, 2014].

Top-of-the-line corrosion (TLC)
Corrosion takes place where there is an accumulation of water. This is typically at the bottom of the pipeline because of gravity. However, in some cases water may condense at the top of the pipeline, causing corrosion. This type of corrosion typically happens in wet-gas pipelines. TLC corrosion could be a big problem because using corrosion-inhibitors will not work in this case. It is usually controlled by applying pipeline insulators to keep the gas from condensing [Papavinasam, 2014].

3.3.3 Important corrosion parameters

There are many parameters used in the modelling of corrosion. The most common parameters are water accumulation, pH, temperature, pressure, flow velocity and presence of mercury.

Water accumulation on metal surfaces is a common cause of corrosion. It is therefore important to locate the places in which water may accumulate. The accumulation of water depends on the geometry of the pipe, flow velocity, oil/gas/water characteristics and pipeline cleanliness [Papavinasam, 2014].

pH is known to be an important parameter in corrosion rate estimation. As the pH decrease there is an increase in corrosion rate. This is because the corrosion layer that is usually formed on the surface is readily dissolved in acidic solution. When the protective layer is removed, further corrosion can occur easily [Papavinasam, 2014].

Temperature has a big effect on corrosion. In most cases an increase in in temperature gives an increase in corrosion rate. Chemical reaction kinetics are generally dependent on temperature, which is also the case for the electrochemical reaction in corrosion. Typically an increase of 10-30°C doubles the corrosion rate. However, this is only applicable in the case of which the corrosion mechanism remains the same. There are some cases where an increase in temperature gives a decrease in corrosion rate. This is because accumulation of water is important for the presence of corrosion. If the temperature is above the dew point the water is not condensed, thus the corrosion rate is decreased. The corrosion rate may also be decreased when the temperature is decreased, not because of kinetics but because of solids formation. This typically happens upon the formation of hydrates, wax and asphaltene [Pantazolpoulos, 1994].

Pressure is an important factor in corrosion. The effect of pressure on corrosion rates depends on the partial pressure of acid gases like H_2S and CO_2, the temperature and pH. High pressure may give a decrease in corrosion rate by causing formation of a compact surface film. However, high pressure may also increase the dissolution of the protective surface film or enhance the dissolution corrosive species in the solution. This will in turn increase the corrosion rate [Pantazolpoulos, 1994].

Flow velocity is also an important corrosion factor. An increase in flow velocity generally gives an increase in corrosion rate, as the corrosive agents are transported faster to the metal surface and the corrosion products are removed from the metal surface [Papavinasam, 2014].

Other factors are also known to influence the corrosion rate. One of these factors is presence of chemical compounds such as organic acids, mercury, glycol O_2, H_2S and CO_2. Microstructure effects, microorganisms, sand and solids and composition of the oil/gas/sand phase are also factors known to affect corrosion [Papavinasam, 2014].

3.3.4 Modelling internal corrosion

Corrosion can happen inside the equipment, but also on the outside. This is called internal corrosion and external corrosion, respectively. This section is focused on internal corrosion, because it is something that is easier to control since we are able to control the content within the equipment. Internal corrosion is caused by presence of CO_2 and H_2S in the fluid.

The models presented in this section are for general corrosion in carbon steel. Unlike the sand erosion models, the rate found in these models are not material removed, but surface material added.

Model by de Waards et. al (1991)

The model by de Waards et al. can be used to predict corrosion rates for sweet corrosion (CO_2 corrosion). It is based on an earlier model by de Waards and Williams. The rate determining step is assumed to be the hydrogen reduction at the cathode. The corrosion rate, C_{corr}, in mm/year can be found from the following equation:

$$\log C_{corr} = 5.8 - \frac{1710}{T} + 0.67 \cdot \log(p_{CO_2}) \tag{3.107}$$

where T is the temperature in K and p_{CO_2} is the CO_2 partial pressure in bar. The corrosion rate can also be found from a nomogram, as shown in Figure

3.19. If the partial pressure of CO_2 is 0.2 bar and the temperature is 120 ° the corrosion rate can be found to be 10 mm/year from the long middle axis. It is however multiplied with a scale factor, which in this case is 0.7, making the predicted corrosion rate 7 mm/year [de Waard et al., 1991].

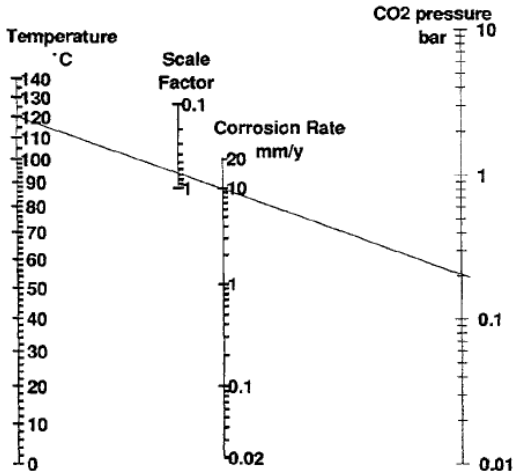

Figure 3.19: Nomogram developed by de Waards and Milliams to predict the corrosion rate. Example: If p_{CO_2} is 0.2 bar and the temperature is 120°C the predicted erosion rate is $10 \cdot 7 = 0.7$ mm/year [de Waard et al., 1991].

If the total pressure is increased, the partial pressure of CO_2 will increase proportionally. In this case, fugacity is used instead of partial pressure to account for non ideal natural gas:

$$\log C_{corr} = 5.8 - \frac{1710}{T} + 0.67 \cdot \log(f_{CO_2}) \tag{3.108}$$

where f_{CO_2} is the CO_2 fugacity:

$$f_{CO_2} = a \cdot p_{CO_2} \tag{3.109}$$

a is the fugacity coefficient which can be estimated from thermodynamic diagrams or mixture state equations. If this is unknown, an estimation of the effect of total pressure can be done:

$$\log F_g = 0.67(0.0031 - \frac{1.4}{T})P \tag{3.110}$$

where F_g is the fugacity coefficient. It is multiplied with C_{corr} from Equation (3.107). This has not been validated against experimental data, but is considered a fundamental effect [de Waard et al., 1991].

At high temperatures ($T > 60°C$) precipitation of $FeCO_3$ and Fe_3O_4 forms a protective film on the material surface. This causes the corrosion rate to decrease. To account for this effect a factor F_{scale} is found:

$$\log F_{scale} = \frac{2400}{T} - 0.6\log(fCO_2) - 6.7 \tag{3.111}$$

F_{scale} has a value between 0 and 1. If F_{scale} is calculated to be > 1, it is set to 1. The factor is multiplied with C_{corr} to account for the effect of protective films. The temperature in which a protective layer begins to form and cause the corrosion rate to decrease is called the scaling temperature. It can be found from:

$$T_{scale} = \frac{2400}{6.7 + 0.6\log(fCO_2)} \tag{3.112}$$

and combined with Equation (3.111) to:

$$\log F_{scale} = 2400\left(\frac{1}{T} - \frac{1}{T_{scale}}\right) \tag{3.113}$$

where $T > T_{scale}$. If the temperature is below the scaling temperature F_{scale} is set to 1. The protective film can be removed at high flow velocities. Wet gas with superficial gas veloctities above 20 m/s is able to remove the scaling. In this case, increasing the temperature will also increase the corrosion rate [de Waard et al., 1991].

Glycol is commonly added to wet gas pipelines to prevent hydrate formation. The glycol absorbs the water from the gas phase and thereby reduces the corrosion rate. The effect of this can be expressed as:

$$\log F_{glycol} = 1.6\log(W\%) - 3.2 \tag{3.114}$$

where $W\%$ is the weight percentage of water in the mixture. F_{glycol} is multiplied with the corrosion rate to account for glycol effects [de Waard et al., 1991].

If the solution is contaminated by Fe^{2+} the factor F_{pH} can be multiplied by the corrosion rate. F_{pH} scan be found from:

$$\log F_{pH} = 0.32(\mathrm{pH}_{sat} - \mathrm{pH}_{act}) \quad \text{for } \mathrm{pH}_{sat} > pH_{act} \tag{3.115}$$

$$\log F_{pH} = 0.31(pH_{act} - pH_{sat})^{1.6} \quad \text{for } pH_{sat} < pH_{act} \tag{3.116}$$

where pH_{sat} is the pH when the solution is saturated, and can be found from

$$pH_{sat} = 1.36 + \frac{1307}{T + 273} - 0.17\log(fCO_2) \tag{3.117}$$

$$pH_{sat} = 5.4 - 0.66\log(fCO_2) \tag{3.118}$$

where the smallest value for pH_{sat} is chosen [de Waard et al., 1991].

The model by de Waard et al. is widely recognized. It is based on experimental data and proven to be a good model when compared to experiments. The experimental values in which the model is based upon and validated against is presented in Table 3.13.

Table 3.13: The experimental data in which the model by de Waard et al. is based upon and validated against [de Waard and Milliams, 1975].

Parameter	Symbol	Experimental range
Temperature	T	5.5 - 80 °C
Partial pressure CO_2	p_{CO_2}	0.21 - 2 bar

Model by Srinivasan (1996)

Srinivasan developed a software to predict the corrosion rate in a system. It is based on the principles of the de Waard et al. model. The advantage of applying a software and computer technology is the ability to perform more calculations and to apply models that are more complex. The equations applied in the software are not presented here, but the corrosion calculation algorithm can be seen in Figure 3.20 [Srinivasan, 1996]s.

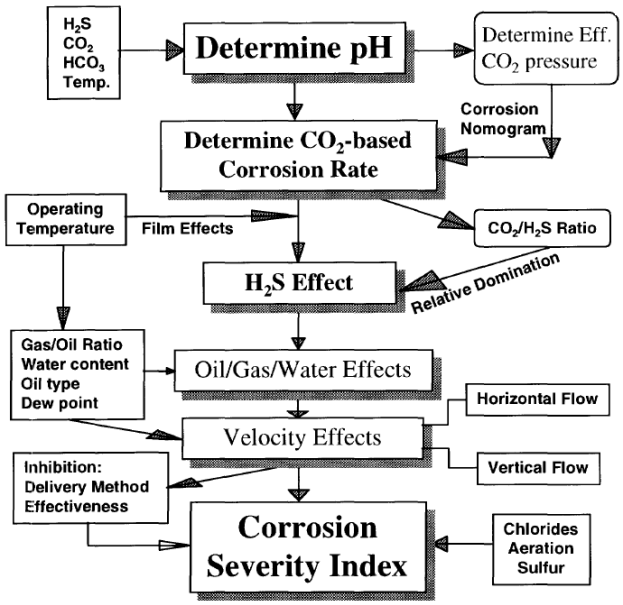

Figure 3.20: The algorithm applied in the software developed by Srinivasan used to predict the corrosion rate [Srinivasan, 1996].

Input parameters in this model are partial pressure of H_2S, CO_2 and HCO_3 and the temperature. The factors considered in this software is pH, surface layer, H_2S, temperature, bicaronate ions, chloride ions, sulfur, ozygen, velocity and oil-gas-water ratio.

Model by Mishra (1997)
The model by Mishra predicts the corrosion rate based on fundamental reaction rate theory. In this model corrosion is considered to be a process controlled by chemical reactions. The corrosion rate, CR, can be estimated from the following equation:

$$CR = a[H^+]^{1.33} \cdot pCO_2^{0.67} \cdot \exp(-\frac{n}{RT}) \tag{3.119}$$

where a is a constant depending on the material, environment and flow velicty, $[H^+]$ is the concentration of hydrogen ions, pCO_2 is the CO2 partial pressure, n is the number of electrons, R is the gas constant and T is the absolute temperature. This model is considered valid up to the point where corrosion is no longer a chemical reaction controlled process, but a diffusion controlled process [Mishra et al., 1997].

Model by Keating and Nesic (2001)
Keating and Nesic developed a model to estimate the corrosion rate based on electrochemical surface reactions and transport processes. CFD was used with a Lagrangian approach to estimate the corrosion rate, assuming that corrosion is controlled by mass transfer. The corrosion rate can be estimated from the following:

$$CR = \frac{2k_m C_{B_{O_2}} M_{Fe}}{\rho_{Fe}} \cdot 86400 \cdot 365 \cdot 10^3 \tag{3.120}$$

where k_m is the wall mass transfer coefficient in m/s, $C_{b_{O_2}}$ concentration of bulk O_2 in mol/m^3, M_{Fe} is the molecular mass of iron in kg/mol and and ρ_{Fe} is the density of iron in kg/m^3 [A. Keating and S. Nesic, 2001].

3.3.5 Modelling corrosion in wellheads

Ossai develoepd a model for predicting corrosion rates in wellheads based on data from oil and gas fields. A model was made based on multiple linear regressions where corrosion rate, CR, in mm/year is expressed as a function

of the operating conditions:

$$CR = f(T, p_{CO_2}, V_m, \text{pH}) \tag{3.121}$$
$$CR = f(T, p_{CO_2}, V) \tag{3.122}$$
$$CR = f(T, p_{CO_2}, V_m) \tag{3.123}$$
$$CR = f(T, p_{CO_2}) \tag{3.124}$$

where T is the temperature in °C, p_{CO_2} is the partial pressure of CO_2 in mpa, V_m is the mixture velocity of the fluid in m/s and V is the flow velocity of crude oil. A linear regression model was applied to model the effect of the parameters:

$$CR = \alpha_{11} + \beta_{11}T + \beta_{12}p_{CO_2} + \beta_{13}V_m + \beta_{14}\text{pH} \tag{3.125}$$
$$CR = \alpha_{21} + \beta_{21}T + \beta_{22}p_{CO_2} + \beta_{23}V \tag{3.126}$$
$$CR = \alpha_{31} + \beta_{31}T + \beta_{31}p_{CO_2} + \beta_{32}V_m \tag{3.127}$$
$$CR = \alpha_{41} + \beta_{41}T + \beta_{42}p_{CO_2} \tag{3.128}$$

where the α and β coefficients can be found from Table A.7 in Appendix A.6.

3.3.6 Erosion - corrosion

Erosion and corrosion are both mechanisms important to equipment degradation, but they can also be combined to give additional degradation effects. Erosion-corrosion is very similar to the corrosive wear mechanism described in Section 3.1.4. Corrosion per se may not be devastating on the equipment. If the layer of corrosion products is not removed by external forces, it will create a protective film that eventually stops corrosion. However, in the erosion-corrosion process, the surface layer is removed by sand particles. The mechanism consists of two steps which are repeated in a loop:

1. Formation of a corrosive layer on the metal surface
2. The corrosive layer is removed by sand particles

Erosion-corrosion seems to be more common in curved equipment such as elbows, tees, valves and pumps than straight pipelines. Today, erosion-corrosion is controlled by increasing the wall thickness at the areas prone to erosion-corrosion and selecting materials that are erosion-corrosion resistant [Papavinasam, 2014].

3.3.7 Modelling erosion-corrosion

This section presents a procedure by Okhovat et al. that can be used to predict the erosion-corrosion in bends.

The erosion-corrosion rate is defined as following:

$$K_{EC} = K_E + K_C \tag{3.129}$$

where K_E is the failure rate due to erosion and K_C is the failure rate due to corrosion. They can be expressed as following:

$$K_E = K_{EO} + \Delta K_E \tag{3.130}$$
$$K_C = K_{CO} + \Delta K_C \tag{3.131}$$

where K_{EO} is the erosion rate in case of no corrosion and ΔK_E is the effect of corrosion on the erosion rate. K_{CO} is the corrosion rate in the case of erosion and ΔK_C is the effect of erosion on the corrosion rate [Okhovat et al., 2014].

Determining K_C
The base for determining K_C is the corrosion rate model by Keating and Nesic that can be found in Section 3.3.4 and Equation 3.120:

$$CR = \frac{2k_m C_{bO_2} M_{Fe}}{\rho_{Fe}} \cdot 86400 \cdot 365 \cdot 10^3$$

The coefficient k_m can be calculated from:

$$k_m = \frac{D}{\Delta y} \frac{C_{fO_2}}{C_b O_2} \tag{3.132}$$

where D is the the mass diffusion coefficient in m^2/s, Δy is the distance of the first cell centre to the wall, C_{fO_2} is the concentration of O_2 in the fluid and C_{bO_2} is the bulk concentration of O_2.

A cylindrical steel pipe where erosion-corrosion has occurred is considered. It is illustrated in Figure 3.21, where r_o is the outer diameter of the pipe, r_i is the inner diameter of the pipe and r_1 is the amount of corrosion in 1 year $= CR^*$.

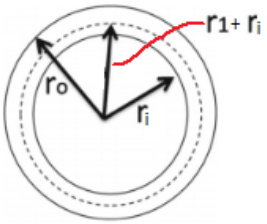

Figure 3.21: A cylindrical pipe where r_o is the outer diameter of the pipe, r_i is the inner diameter of the pipe and r_1 is the amount of corrosion in 1 year = CR^* [Okhovat et al., 2014]

The removed volume because of erosion-corrosion is given by:

$$V = \pi \cdot L((r_i + r_1)^2 - r_1)^2 = \pi L(2r_i CR^* + CR^{*2}) \tag{3.133}$$

where L is the length of the cylinder [Okhovat et al., 2014].

The area exposed to corrosion is [Okhovat et al., 2014]:

$$A_{corr} = 2\pi r_i L \tag{3.134}$$

The total wear rate due to corrosion can be found from dividing the removed volume by the area exposed to corrosion. It is multiplied with the density of steel, ρ_{steel} so that the unit is in kg/m^2. The result is as following:

$$K_C = \frac{\rho_{steel}(2r_i CR^* + CR^{*2})}{2r_i} \tag{3.135}$$

Determining K_E
The base for determining K_E is the erosion model by Sundararajan and Shewmon that can be found in Section 3.2.3 and Equation 3.100:

$$\epsilon_s \approx \frac{6.5 \cdot 10^{-3} V_p^{2.5} \rho_p^{0.25}}{C_p T_m^{0.75} H_t^{0.25}}$$

To determine K_E it is multiplied with the particle flux rate in g/m^{2}h:

$$F = 3.6 \cdot 10^9 c V_p \tag{3.136}$$

where c is the particle concentration and V_p is the particle velocity particles [Okhovat et al., 2014].

K_E is then found to be:

$$K_E = \epsilon_s \cdot F = \frac{2.34 \cdot 10^7 \rho_p^{0.25} c V_p^{3.5}}{C_p T_m^{0.75} H_t^{0.25}} \tag{3.137}$$

Determining K_{EC}
Inserting Equation (3.135) and Equation (3.137) into Equation (3.129) gives the following erosion-corrosion rate:

$$K_{EC} = \frac{2.34 \cdot 10^7 D_p^{0.25} c v^{2.5}}{C_p T_m^{0.75} H_s^{0.25}} + \frac{\rho_{steel}(2 r_i CR^* + CR^{*2})}{2 r_i} \tag{3.138}$$

It was found that this model agreed well with experimental data [Okhovat et al., 2014]. The test conditions of the experiment that the model results are compared to are shown in Table (3.14).

Table 3.14: The test conditions in the experiment in which the model results were compared to [Lotz and Postlethwaite, 1989].

Parameter	Test conditions
Pipe diameter	21 - 42 mm
Length of construction	222 mm
Fluid velocity	3.3 - 13.2 m/s
Average particle diameter	430 μm
Particle concentration	0 - 2 w%
Temperature	30 °C
Time	48 h
NaCL concentration	3 wt%
Pressure	1 atm

4 Failure information databases

There are many databases for accidents and incidents in the oil and gas industry. Sets of information from these databases could be useful when developing models for failure mechanisms in subsea equipment.

It is important that the failure information generally is reported in the same manner. ISO 14224 is an International Standard written for the petroleum and gas industry regarding the collection and exchange of reliability and maintenance data for equipment. It is based on the data collection project OREDA in addition to know-how. Such a standard is necessary to be able to collect, analyze and exchange data [ISO, 2006]FOREDA.

Four databases are presented in this section: OREDA, WOAD, HCR and "Hendelsesdatabasen".

4.1 OREDA

The Offshore and Onshore Reliability Data (OREDA) database is a collaboration between eight oil and gas companies. The purpose is to store and exchange reliability data. The database contains comprehensive information about a wide range of equipment and operating conditions. It is however closed for the public and special licences are needed to access the database [DNV-GL, 2014].

4.2 WOAD

The Worldwide Offshore Accident Databank (WOAD) is the most comprehensive database with more than 6000 events dating back to 1970. The data is collected from reports, publications, newspaper and from authorities. There are some limitation in how detailed the descriptions of the accidents are. This database is available for the public for an annual fee [DNV-GL, 2014].

4.3 HCR

The Hydrocarbon Releases (HCR) database contains information about all hydrocarbon releases that has voluntarily been reported to the Health and Safety Executive in UK. However, information about leaks from subsea facilities is limited and the database is generally not available for the public [DNV-GL, 2014].

4.4 "Hendelsesdatabasen"

"Hendelsesdatabasen" (the incident database) is operated by the Petroleum Safety Authority Norway. It contains information about hydrocarbon leaks on the Norwegian continental shelf. It is hard to tell the root cause of the incidents based on the information available. The database also does not seem easily available to the public [DNV-GL, 2014].

5 Case study: a simple production system

A case study has been performed to explore how the knowledge obtained from the literature study can be applied on subsea production systems. This is an example of how failure mechanism models may be applied in failure rate and residual lifetime estimations for a system.

5.1 System description

The following system has been designed: Two 5" pipelines emerge from a reservoir. Each pipeline has a choke valve to control the flow of fluid from the reservoir. Downstream of the choke valve each pipeline has an elbow. The pipelines are joined into a 7" pipeline, which also has an elbow. The system is illustrated in Figure 5.1. The blue numbers represent the pipeline number.

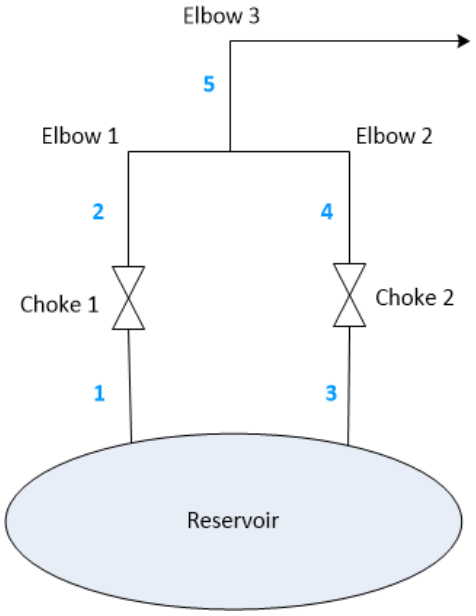

Figure 5.1: System applied in the case study. Two 5" pipelines with a choke valve emerge from the reservoir. Both pipelines have an elbow and they are joined in a 7" pipeline that also has an elbow. The blue numbers represent the pipeline number.

The only failure mechanism that has been considered in this case study is sand erosion. This is because the literature review revealed that this is a common and important failure mechanism in subsea equipment, there are many models and data connected to sand erosion, the mechanism of is well

known and the effect of the different parameters on the erosion rates are also well known.

Sand erosion has been modelled and simulated for the two choke valves and the three elbows.

5.2 Assumptions

In this simplified case study the following assumptions are made:

- The only possible failure mechanisms in this system is sand erosion in the elbows and the choke valves.
- The equipment is considered to be failed when the wall thickness is reduced to 0 mm.
- The inner dimensions of the equipment are considered constant, even though the erosion is removing material from the equipment walls.
- The sand production rate is evenly distributed between the two emerging pipelines, which means the mass rate of sand is the same in both pipelines.
- The oil and gas flow rate are mostly treated as constant.
- The density and viscosity of the gas across the valves are constant.
- The sand particles are not degraded in any way once they hit a surface. No energy is lost in the impact and equipment downstream may be hit by the same particle.
- The sand particles are assumed to be semi-rounded, $F_S = 0.53$.
- The equipment material is assumed to be carbon steel, $F_M = 1.95 \cdot 10^{-5}/B^{-0.59}$.
- The radius of curvature, r_c, in the bends are set to 1.5.
- The lifetime of the field/system is set to 30 years.

5.3 Model implementation

To estimate the erosion rate in the elbows and choke valves, the different models described above were used. The implementation of the different models is presented in this section.

5.3.1 Erosion in elbows

To estimate the erosion in the bends, McLaury's multi-phase erosion model from Section 3.2.3 was applied. This model was chosen because it is quite detailed without being too complicated. A certain level of detail in the model was wanted in order to be able to play around with some of the variables. Also, if the model is to be used for later purposes, this could give advantages compared to a simpler model. The model by McLaury was one of the most detailed model found in the literature review that did not take into account different flow patterns. This was also wanted because of the extra level of complexity to the work.

The script used to calculate this can be found in Appendix C.3. The factors used in the script can be found in Table 5.15.

Table 5.15: Factors used in the model by McLaury et al. to calculate the erosion rate in elbows.

Factor	Symbol	Value
Material factor	F_m	$1.62 \cdot 10^{-7}$
Sharpness factor	F_s	0.53
Penetration factor	F_p	0.206 m/kg
Reference diameter	D_{ref}	1 inches
Radius of curvature	r_c	1.5

5.3.2 Erosion in choke valves

To estimate the erosion in the choke valves, the choke valve model by DNV-GL from Section 3.2.4 was used. It was chosen for the same reasons as McLaury's multi-phase model for elbows. The model by DNV-GL is quite detailed compared to the model by Haugen et al., and like the model by McLaury it does not get into various flow patterns.

The script used to estimate the erosion in the choke valves can be found in Appendix C.2. The factors and parameters used in the script can be found in Table 5.16.

Table 5.16: Factors and parameters used in the choke erosion model by DNV-GL.

Factor/parameter	Symbol	Value
Unit conversion factor	C_{unit}	$3.15 \cdot 10^{10}$
Model/geometry factor	C_1	1.25
Material erosion constant	K	2.00E $\cdot 10^{-9}$ $(\mathrm{m/s})^{-n}$
Density carbon steel	ρ_t	7 800 $\mathrm{kg/m^3}$
Velocity coefficient	n	2.6
Geometry factor	GF	2
Radius of curvature	r	0.25 m
Gas between body and cage	D	0.10 m
Height of the gallery	H	0.40 m

5.3.3 Valve equations

To model the mass flow, $\dot{m}$, across a valve, the following equation can be used:

$$\dot{m} = f(z)C_d A\sqrt{\rho(P_2 - P_1)} \tag{5.1}$$

where $f(z)$ is the valve characteristic function, C_D is the valve constant, A is the cross sectional area, ρ is the density of the fluid and P_1 and P_2 are the pressures before and after the valve, respectively. The valve characteristic function is assumed to be linear:

$$f(z) = z \tag{5.2}$$

where z may have values from 0 (fully closed) to 1 (fully open) [Grimholt and Skogestad, 2015].

5.4 Simulations

Multiple simulations have been performed to investigate the erosion in this subsea production system. At first, a base case simulation is presented to show how the various equipment deteriorate under nominal conditions. A parameter study has also been performed on the system, to see how the liquid and gas velocities in the flows affect the estimated lifetime.

5.4.1 Basic case

The first simulation for the base case is set up to see how the system components behave generally. The parameters applied in the base case can be seen in Table 5.17.

Table 5.17: Parameters used in the base case simulation.

Parameter	Symbol	Value
Sand production rate	m_p	$2.00 \cdot 10^{-4}$ m^3/s
Density gas	ρ_g	100 kg/m^3
Density liquid	ρ_l	$1.5 \cdot 10^{-5}$ kg/m^3
Viscosity gas	μ_g	800 kg/ms
Viscosity liquid	μ_l	$2 \cdot 10^{-3}$ kg/ms
Particle diameter	d_p	$2.50 \cdot 10^{-4}$ m
Particle density	ρ_p	$2.50 \cdot 10^{-3}$ kg/m^3

The flow parameters used in this case are listed in Table 5.18. The total flow is the same in each stream, but the composition is not the same. This has been done to see how different compositions affect erosion rates.

Table 5.18: The flow parameters used in the base case.

Parameter	Symbol	Value
Liquid volumetric flow 1	Q_{L1}	0.1 m^3/s
Gas volumetric flow 1	Q_{G1}	0.5 m^3/s
Liquid volumetric flow 2	Q_{L2}	0.3 m^3/s
Gas volumetric flow 2	Q_{G2}	0.3 m^3/s

The following definition of the flows is used throughout the rest of the report:

$$\begin{aligned} \text{Flow 1} &= (1) + (2) \\ \text{Flow 2} &= (3) + (4) \\ \text{Flow 3} &= (5) \end{aligned}$$

where (1), (2), (3), (4) and (5) are the pipeline numbers as described in Figure 5.1.

The flow rates in Flow 3 were found from the following equations:

$$Q_{L3} = Q_{L1} + Q_{L2} \tag{5.3}$$
$$Q_{G3} = Q_{G1} + Q_{G2} \tag{5.4}$$

The sand flow rate in Flow 3, m_{p3}, is also calculated:

$$m_{p3} = m_{p1} + m_{p2} \tag{5.5}$$

The erosion rates in the equipment for this case was found using the MATLAB scripts in Appendix C.1. The results are presented in Table 5.19.

Table 5.19: The erosion rates found for each equipment in the base case.

Equipment	Erosion rate
Elbow 1	0 mm/year
Elbow 2	0.2095 mm/year
Elbow 3	0.0165 mm/year
Choke 1	0.9030 mm/year
Choke 2	0.4493 mm/year

A wall thickness of 10 mm was assumed for both choke valves and pipelines. The erosion rate is constant, hence there is a linear degradation of the wall:

$$w_{i,r} = w_{(i-1),r} - ER_r \tag{5.6}$$

where w is the thickness of the wall of equipment r in year i, $w_{(i-1),r}$ is the thickness of the wall of equipment r the previous year and ER_r is the erosion rate in equipment r. The thickness of the wall as a function of the time is shown in Figure 5.2. The time scope has been set to 30 years, which is the estimated lifetime of the field.

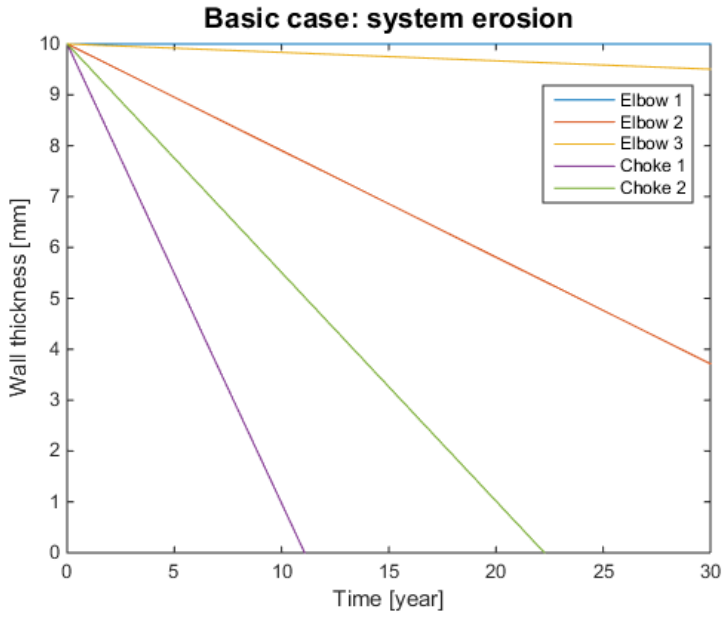

Figure 5.2: Results of simulating in the base case. The thickness of the wall is plotted as a function of the time for the three elbows and the two chokes.

As can be seen from Figure 5.2, under the conditions given in Table 5.17 and Table 5.18, Choke 1 is the first equipment to fail, after approximately 11 years. Both choke valves will have to be replaced if this was the case, as the field lifetime is 30 years.

5.4.2 Parameter studies

The effect of the different parameters on the equipment lifetime has also been explored. Various flow rates from 0.1 m^3/s to 1.0 m^3/s are applied in intervals of 0.1 to the flow parameters Q_{L1}, Q_{G1}, Q_{L2} and Q_{G2} to see the effect on erosion rate and estimated equipment lifetime. The erosion rates are found in the same way as in the base case, by the erosion models by McLaury and DNV-GL. The parameters from Table 5.17 are still applied.

To find the estimated equipment lifetime, Equation (5.6) is applied in a *while-loop* with a counter. As long as the wall thickness is still above zero (equipment not failed) an iteration is done and another year is added to the lifetime counter. The estimated lifetime is plotted against the flow rate. Variations of the MATLAB script in Appendix is used for this calculation C.4.

The field lifetime is set to 30 years. When the erosion rates are very low (or zero), the estimated lifetime will be very high. Cases where the equipment is not estimated to fail within the field lifetime has not been included in the graph.

The effect of Q_{L1} on failure rates and estimated lifetime

The effect of increasing the liquid velocity in Flow 1, Q_{L1}, on the estimated lifetime of the system components has been simulated. Estimated erosion rates and estimated lifetimes of the equipment can be found in Table A.8 and Table A.9, respectively. Figure 5.3 shows how the equipment lifetime is affected by changes in the liquid velocity in Flow 1.

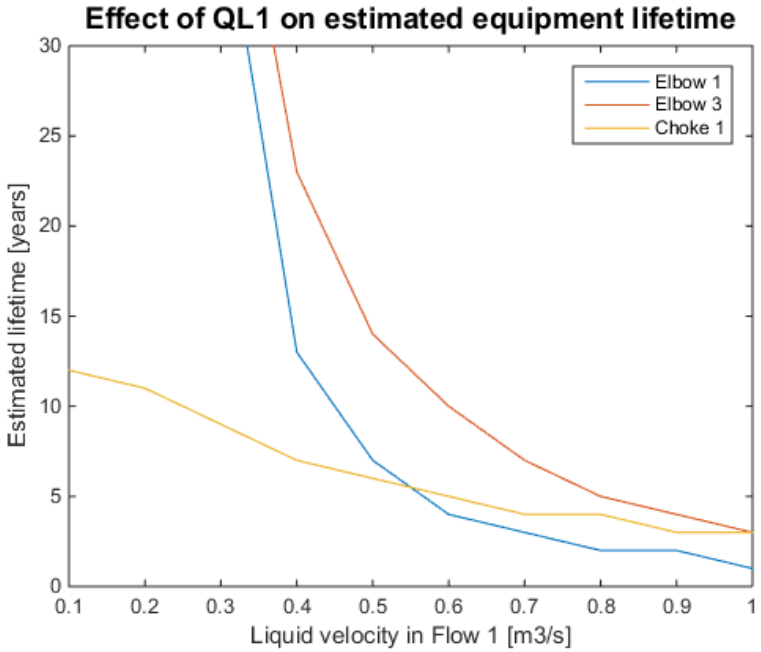

Figure 5.3: The estimated lifetime of the equipment in the system at different liquid velocities in Flow 1, Q_{1L}. This plot was made using a version of the MATLAB script in Appendix C.4.

The effect of Q_{G1} on failure rates and estimated lifetime

The effect of increasing the gas flow in Flow 1, Q_{G1}, on the estimated lifetime of the system components has been simulated. Estimated erosion rates and estimated lifetime of the equipment can be found in Table A.10 and Table A.11, respectively. Figure 5.4 shows how the equipment lifetime is affected by changes in the gas velocity in Flow 1. Elbow 1 is not included, as the erosion rate is 0 mm/year for most gas velocities. It is not expected not fail due to erosion within the lifetime of the field.

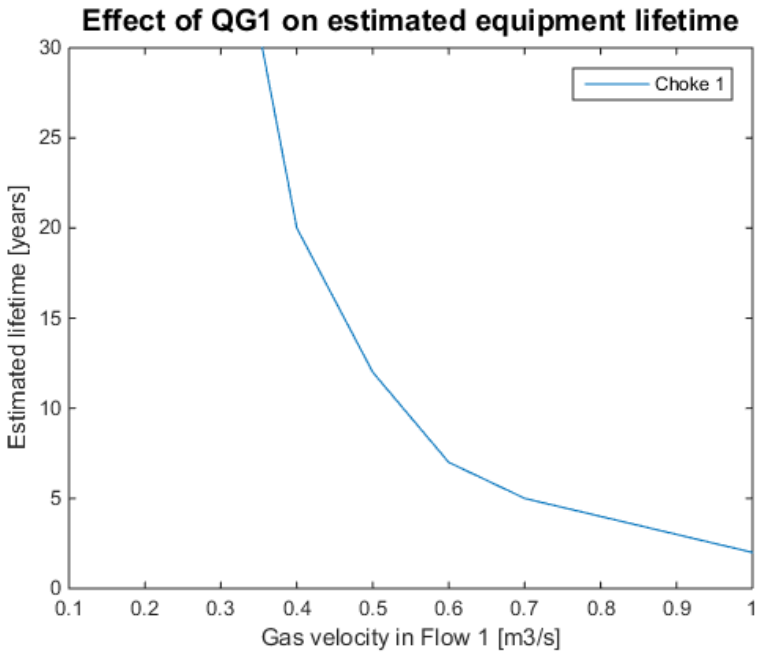

Figure 5.4: The estimated lifetime of the equipment in the system at different gas velocities in Flow 1, Q_{G1}. This plot was made using a version of the MATLAB script in Appendix C.4.

The effect of Q_{L2} on failure rates and estimated lifetime

The effect of increasing the liquid velocity in Flow 2, Q_{L2}, on the estimated lifetime of the system components has been simulated. Estimated erosion rates and estimated lifetimes of the equipment can be found in Table A.12 and Table A.13, respectively. Figure 5.5 shows how the equipment lifetime is affected by changes in the liquid velocity in Flow 2.

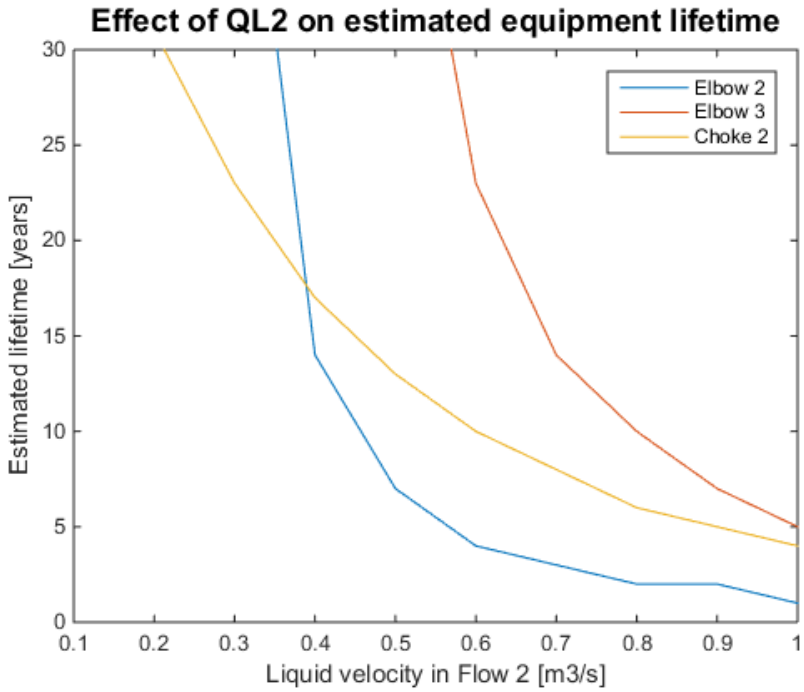

Figure 5.5: The estimated lifetime of the equipment in the system at different liquid velocities in Flow 2, Q_{L2}. This plot was made using a version of the MATLAB script in Appendix C.4.

The effect of Q_{G2} on failure rates and estimated lifetime
The effect of increasing the gas flow in Flow 2, Q_{GL2}, on the estimated lifetime of the system components has been simulated. Estimated erosion rates and estimated lifetimes of the equipment can be found in Table A.14 and Table A.15, respectively. Figure 5.6 shows how the equipment lifetime is affected by changes in the gas velocities in Flow 2. Elbow 3 is not included, as the estimated lifetime for all Q_{G2}s in the range of 0.1 m^3/s to 1.0 m^3/s is greater than the estimated lifetime of the field.

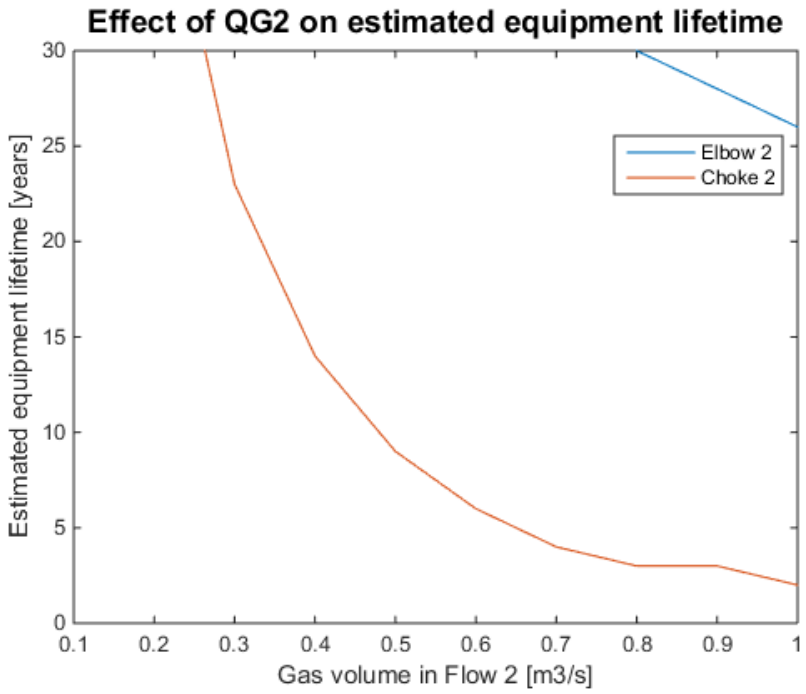

Figure 5.6: The estimated lifetime of the equipment in the system at different gas velocities in Flow 2, Q_{G2}. This plot was made using a version of the MATLAB script in Appendix C.4.

6 Discussion

6.1 Failure mechanism models

6.1.1 Using already existing failure models

Many models were found in the literature review, and a selection of them are presented in this thesis.

First, the mechanical wear mechanisms were presented. The mechanical wear models are very basic and for equipment with multiple components they may be too simple for application. However, they seem to be a good starting point for developing theoretical models for various wear mechanisms. It is also interesting to note that both the abrasion and adhesion mechanism can be recognized in sand erosion. In this case, the sand particle acts as one of the contact surfaces.

The section about sand erosion is quite extensive, because many models were found for this mechanism. The models presented are empirical, mechanistic or CFD-based. CDF-based models give the opportunity to do advanced calculations with more model parameters, but the main focus has been on empirical and mechanistic models because they are easier to apply. There are great amounts of experimental data on sand erosion, which is an advantage when doing modelling, as it gives an opportunity to properly validate the model results.

The corrosion mechanism also had quite a lot of models, but they generally seem more complicated than what was found for sand erosion. In addition to the fluid and wall properties that were included for sand erosion, chemical properties like potential and pH are also important. in corrosion It seemed like more often CFD-based models or software programs were used to estimate corrosion rates.

6.1.2 Using databases in the development of new models

Section 4 presents some of the major failure databases within the oil and gas industry. It is a possibility to use the information stored within these databases to develop new failure models for subsea equipment. The accuracy of such a model would depend on the type, quality and amount of data stored.

One big issue is that the databases are rarely available for the public and special licences are needed to access them. Also, it should kept in mind that

data from the early years may not be relevant for the failure models today, as technological advances have improved the equipment reliability over the years.

6.2 Simulations

Several simulations were performed to explore erosion modelling in multi-component systems. Doing simulations is both a way to see how the system behaves, but also a way to assess if the implemented models are applicable through comparing the simulated results to the expected results based on knowledge of the mechanism.

6.2.1 Base case

In the base case, degradation of the equipment walls as a function of time was modelled. Different values were set for the liquid and gas velocities in Flow 1 and Flow 2, to see how this affects degradation in the system components.

From Figure 5.2 it can be seen that Choke 1 is predicted to fail first, after $\approx$ 11 years. The next equipment to fail is Choke 2 after $\approx$ 22 years. Both streams have the same total volumetric flow $V_{total} = V_{liquid} + V_{gas} = 0.6$ m^3/s, but the gas/liquid composition is different. Choke 2 has smaller liquid flow and greater gas flow than Choke 1. This gives a lower mixture density and mixture viscosity. As mentioned in Section 3.2.2, highly viscous fluids may slow sand particles down and reduce the erosion rate. It is therefore reasonable that the choke with the lowest viscosity (Choke 1) experience the greatest erosion damage.

There was no predicted erosion in Elbow 1. This is probably because of the low liquid velocity in Flow 1. In the model applied to estimate the erosion rate in elbows, the initial velocity of the particle was set equal to the liquid velocity. As a result of the low particle initial velocity, the particle velocity at the wall could be zero. In other words, there would be no particle impact on the wall. The erosion rate in Elbow 3 was estimated to be 0.0165 mm/year, which is so low that the wall decrease of wall thickness hardly shows in the figure. The failure rate in Elbow 2 was estimated to be quite high, but not high enough to expect a failure in the time scope of 30 years.

The choke valves having higher erosion rates than the elbows could also reasonable, considering choke valves are usually more prone to erosion than elbows [Barton, 2003]. Based on this simulation the results seem to be as

expected, and it is reasonable to think that the model is working correctly to give a decent image of reality.

6.2.2 Parameter study

In the parameter study, the liquid and gas velocities of Flow 1 and Flow 2 were changed on3 at a time while keeping the other parameters constant. The results are shown in Figure 5.3 - Figure 5.6 and Table A.8 - Table A.15.

In Figure 5.3 the estimated lifetime of the system components as the liquid velocity in Flow 1, Q_{L1} changes is shown. It can be seen that for low liquid flow rates, the equipment estimated to fail first is Choke 1. However, at some point between $Q_{L1} = 0.5$ m^3/s and $Q_{L1} = 0.6$ m^3/s, which equipment estimated to fail first changes. Now Elbow 1 is the new equipment estimated to fail first. A change like this also occured in Figure 5.5, where the parameter Q_{L2} is changed.

It might appear from Figure 5.3 that the lifetime of the choke and elbow completely flattens out at some high velocity regions. The is because of the way the MATLAB script works. For each iteration, one year is added to the timeline. What time of the year the equipment fails it not taken into consideration. Even though they are estimated to fail the same year they will probably not fail at the same time of the year. If a smaller time scale was to be applied, these completely flat regions would probably disappear. For application in process control, a smaller time scale than years would probably be preferred.

This result very interesting in respect to process control and optimization opportunities. A control structure in this system can give the opportunity to actively control which equipment in the same production line is most prone to erosion. If the equipment were to fail purposely at the same time, maintenance could be performed in both the choke valve and elbow simultaneously, which is beneficial if the production in that pipeline must be stopped in order to perform maintenance. Or, maybe the cost of replacing one equipment is much larger than the other, adding another factor to the optimization problem. Cost of maintenance, cost of production and revenue from production go into an optimization problem, to find the optimal maintenance strategy with respect to economics and system degradation.

However, there is a possibility that this is not a correct result. According to literature, choke valves are more prone to erosion than elbows [Barton,

2003]. Under the same conditions, a choke valve will generally fail before an elbow. No experiments where erosion rates for choke valves and elbows for the same conditions have been found. It is therefore difficult to validate this result.

It is peculiar that this only happens when the liquid velocity is changed. It draws the attention to the differences in the model by McLaury and model by DNV-GL, making it a possibility that the two models should not be used together as they could have different ranges of validity. In the model by McLaury, which is used to calculate the erosion rate of elbows, it is assumed that the initial velocity of the particle equals the liquid velocity. The particle is then decelerated as it approaches the wall, giving a lower impact velocity. In the DNV-GL model, the impact velocity equals the mixture velocity $V_p = V_m = V_l + V_g$. For constant values of V_g, the impact velocity will be bigger in the DNV-GL model. Due to this difference in impact velocity calculation, but also difference in factors and range of validity, it is hard to compare the models.

It is also important to remember that these models are only a representation of the reality. They both have an area of validation, and outside this area they may not be applicable at all. Also, within the area of validation there is an uncertainty due to factors like measurement error and random noise. Upon further investigation, the superficial liquid velocity in the simulation was found to be $>> 6.2$ m/s which is the upper experimental range of which the McLaury model is validated against. Care should be taken when extrapolating parameters like this, and it could definitely give faulty results. The parameters are well within the range of the DNV-GL model, but it is stated in their Recommended Practice that the model for choke valves are quite uncertain due to the complex geometry of the choke valves. In the end, without the opportunity to validate this result it is hard to know either way which is true. It remains a strong possibility that the result is not physically correct.

Figure 5.4 shows how the estimated lifetime of the system components is affected by changes in the gas velocity in Flow 1. As can be seen from the figure, the simulated change in Q_{G1} only affects Choke 1. At high gas velocities it is estimated to fail quite fast. This seems reasonable, as the high gas velocities give higher impact velocities.

In Figure 5.5 the estimated lifetime of the system components as the liquid velocity in Flow 2 changes is shown. Both Choke 2, Elbow 2 and Elbow 3 are affect by changes within the velocity range applied in the simulation. A

switch in which equipment is expected to fail first occurs at $\approx Q_{L2} = 0.4$ m^3/s.

Figure 5.6 shows how the estimated lifetime of the system components is affected by changes in the gas velocity in Flow 2, Q_{G2}. At high gas velocities ($Q_{G2} > 0.8$), Elbow 2 is predicted to fail within the lifetime of the field. This seems reasonable because the increased gas fraction will cause lower viscosity and density, and thus higher particle impact angle.

6.2.3 Implementing valve equations

Due to time limitations, the valve equation was not implemented in the simulations. Nevertheless it deserves a short mention in the discussion.

There is always a pressure drop over a valve, and thus there must always be a change in the gas density. This has been neglected in this case study. This is a big simplification, and for the base simulations of this case study it is probably OK. If these models are further developed to process control purposes, the valve equations should be implemented to give a better accuracy and better control. The change of density is quite important for the estimation of erosion rates, as it affects the fluid and particle movement.

If the valve equation is implemented, the erosion rate could be controlled by adjusting the valve opening and thus the mass flow across the valve. This could give the opportunity to apply process control in order to optimize the system for maintenance and economics. One possible issue by implementing valve equations is the potential change in flow pattern. In this case, flow patterns are not taken into account. However, if they were, different erosion models may have to be applied for different valve openings. This adds a lot of extra work to the modelling.

6.2.4 Considering the assumptions

The first assumption is that the only failure mechanism in this system is sand erosion. This is most likely not a correct assumption, as most production systems experience a lot of corrosion. How this will affect the outcome of the simulations is hard to say, but the erosion rates would probably be higher and the estimated lifetimes lower. This is because due to the corrosive layer being easier to remove than the ordinary material surface.

The second assumption is that the equipment is considered to be failed when

the equipment wall thickness is reduced to 0 mm. This is also not quite correct, as it is likely that the equipment would collapse because of the reduced wall thickness before a hole has been made in the pipe. A better approach may be to determine a critical wall thickness in which the equipment will fail, either based on mechanical strength calculations or simplified as a percentage of the wall thickness. This assumption could give a longer estimated lifetime than what is true, which is highly unwanted when predicting failures.

It was assumed that the inner dimensions of the equipment were constant, which obviously is not true when the walls are eroded. However, the change in wall thickness is so small (up to 10 mm) compared to the inner diameter of the pipes (minimum 127 mm), so this should not cause any problems in the case study.

Another assumption that was made is that the sand production rate is evenly distributed and constant throughout the field lifetime. This is usually not the case in real life. The composition of the reservoir will probably change during the field lifetime. A similar assumption that was made is that the oil/gas flows stay constant throughout the field lifetime. This is not at all the case, and as the mass flow of oil/gas is changed, the mass flow of sand is probably affected as well. Making these assumptions is most likely not a big problem in this simple case study. However, if it was to be expanded, this should probably be dealt with.

It was assumed that the sand particles are not degraded or losing energy at the moment of impact. This is a simplification that is not physically correct. The result of this assumption is probably an overestimation of erosion rates. An alternative would have to run a calculation on how much energy was lost in the impact. A certain percentage loss can also be assumed. Loss of energy is slightly mentioned in Section 3.2.3 in Equation (3.98) and Equation (3.99), where the velocity before and after impact is used to find restitution coefficients.

It was also assumed that the density and viscosity remain constant across the valve, which is not correct. The driving force of the stream is the pressure difference across the valve, which means that if there were not pressure difference there would be no flow. Viscosity and density are properties that are very dependent on pressure, which means that this assumption could cause problems in the simulation. The next step of the simulation was to implement the valve equations to account for this, but due to time limitations it was not performed. It remains a recommendation for further work.

The last assumptions were made for equipment and sand characteristics such as shape of the particles, material of the equipment, radius of curvature and field lifetime. The correctness of these assumptions depend on the system, but changes are easy to implement. This should not cause any trouble in the simulation.

To conclude, many assumptions were made in this case study. Some should give an overestimation of erosion/failure rates while others give an underestimation. It is hard to say if the final calculations are too high, too low or quite right. Removing some of the assumptions could help clarify this.

6.2.5 Treating failure as a deterministic variable

In real life there are many failure mechanisms happening at the same time in a system. Some of them are affecting each other, such as erosion and corrosion. Additionally, even a simple system may consist of a huge amount of smaller parts, and each part may multiple things that can go wrong. In the end, there are so many things going on and because of the complexity and uncertainty in the system, failures may be considered to have a stochastic (random) element of them.

Failure has been treated as a deterministic variable in this case study. Because of the simple nature of this case, it is probably OK. Generally it can be problematic because the random nature of risk is left out. In the RAMS field, risk is typically treated as a stochastic variable. As briefly mentioned in the introduction, an attempt to combine the methods of RAMS and process control/optimization is yet to be made. If however a stochastic element was added to this system, it would be a first step. This is something that should be tested in further work.

7 Conclusion

The oil and gas industry is recently facing a challenge to increase the efficiency and reduce the costs. One way to reduce costs is to better optimize the maintenance strategy. Performing maintenance in subsea environments can be challenging because of harsh environmental conditions. By applying failure mechanism models it could be possible to predict equipment degradation rates and estimate the remaining equipment lifetime based on some controllable input parameters. The operation could then be optimized for maintenance, safety and cost, which would be beneficial for both the company and the environment.

A literature review was performed in order to get an overview of important failure mechanisms in subsea equipment and how they can be modelled. The most common subsea equipment has been described along with their common failure mechanisms. A wide variety of failure mechanisms was discovered. The most common failure mechanisms in subsea equipment were found to be sand erosion, corrosion and mechanical failure. Each of these failure mechanisms have been described in detail, along with how they can be modelled. Some failure databases have also been investigated, as they may be used to develop failure models in the future.

A base case was simulated to see how some of the failure models could be applied in a simple subsea production system. In the case study, the main focus was sand erosion in elbows and choke valves. Finally, a parameter study was performed to see how changes in the liquid and gas velocities would affect failure rates and estimated lifetime of the elbows and chokes. The simulations usually gave reasonable results. As the liquid and gas velocity increased, the failure rate increased and the estimated lifetime decreased as expected. For high values of liquid velocity, the elbows were estimated to have a shorter lifetime than the choke valves, which is the opposite of what was found in the literature review. A possible reason for this could be that the sand erosion model was extrapolated in this area, and this could give faulty results. Within the validity range of the model the results seemed to be what was expected.

The final conclusion is that it is indeed possible to model failure mechanisms in a system with process control and optimization in mind. It is recommended that the model used in this case is further developed before used in this application, because there are many elements of uncertainty.

7.1 Further work

Recommendations for further work is to improve the model by implementing the valve equation, so that pressure drop and change in gas density and viscosity is included in the model. Other assumptions could also be dealt with, such as the assumption that the sand production rate is constant.

Other failure mechanisms could be implemented in the model as well, such as corrosion and the effect of erosion-corrosion. Another option is to add a stochastic element to the model to account for the random nature of risk in a system and in an attempt to build a bridge towards the stochastic methods of RAMS.

References

[4subsea, nd] 4subsea (n.d.). System Engineering. http://www.4subsea.com/services/flexible-risers/system-engineering. Accessed: 05.05.2016.

[A & W Compressor, nd] A & W Compressor (n.d.). Reciprocating Compressor Sales and Service from Nashville to Knoxville and Throughout Tennessee. http://www.awcompressor.com/reciprocating-compressor.html. Accessed: 05.05.2016.

[A. Keating and S. Nesic, 2001] A. Keating and S. Nesic (2001). Numerical prediction of erosion-corrosion in bends.

[Adkins, 2012] Adkins, M. D. (2012). Matching valve type to function: a tutorial in valve selection.

[American Petroleum Institute, 1991] American Petroleum Institute (1991). Api recommended practice 14e (rp 14e).

[Bai and Bai, 2005] Bai, Y. and Bai, Q. (2005). Subsea Pipelines and Risers. Mechanics of Offshore Pipelines. Elsevier Science, Burlington.

[Bai and Bai, 2012] Bai, Y. and Bai, Q. (2012). Subsea Engineering Handbook.

[Barton, 2003] Barton, N. A. (2003). Erosion in elbows in hydrocarbon production systems: Review document.

[Bellman and Levy, 1981] Bellman, R. and Levy, A. (1981). Erosion mechanism in ductile metals. Wear, 70(1):1–27.

[Bhushan, 2000] Bhushan, B. (2000). Modern Tribology Handbook, Two Volume Set. CRC Press.

[Brondel et al., 1994] Brondel, D., Edwards, R., Hayman, A., Hill, D., Mehta, S., and Semerad, T. (1994). Corrosion in the oil industry.

[Challen et al., 1986] Challen, J. M., Oxley, P. L. B., and Hockenhull, B. S. (1986). Prediction of archard's wear coefficient for metallic sliding friction assuming a low cycle fatigue wear mechanism. Wear, 111(3):275–288.

[Chen et al., 2005] Chen, X., McLaury, B. S., and Shirazi, S. A. (2005). A comprehensive procedure to estimate erosion in elbows for gas/liquid/sand multiphase flow. Journal of Energy Resources Technology, 128(1):70–78.

[Colorado Geological Survey, nd] Colorado Geological Survey (n.d.). Corrosive Soil Damage. http://coloradogeologicalsurvey.org/geologic-hazards/corrosive-soils/corrosive-soil-damage/. Accessed: 20.05.2016.

[Dale et al., 2013] Dale, N., Heskins, D., and Bolton, M. (2013). Wellhead maintenance & integrity management.

[de Waard and Milliams, 1975] de Waard, C. and Milliams, D. E. (1975). Carbonic acid corrosion of steel.

[de Waard et al., 1991] de Waard, C., U.Lotz, and Milliams, D. E. (1991). Predictive model for co2 corrosion engineering in wet natural gas pipelines.

[Desale et al., 2009] Desale, G. R., Gandhi, B. K., and Jain, S. C. (2009). Particle size effects on the slurry erosion of aluminium alloy (aa 6063). Wear, 266(11):1066–1071.

[DNV-GL, 2014] DNV-GL (2014). Subsea facilities - technology developments, incidents and future trends.

[DNV-GL, 2015a] DNV-GL (2015a). 2628 Introduction to subsea production systems.

[DNV-GL, 2015b] DNV-GL (2015b). Managing sand production.

[Febo and Paganini, 2016] Febo, M. D. and Paganini, P. (2016). Efficiency improvement in centrifugal pumps.

[Finnie, 1960] Finnie, I. (1960). Erosion of surfaces by solid particles. Wear, 3(2):87–103.

[Gandhi and Borse, 2002] Gandhi, B. K. and Borse, S. V. (2002). Effects of particle size and size distribution on estimating erosion wear of cast iron in sand-water slurries.

[Gomez et al., 2000] Gomez, L., Shoham, O., and Taitel, Y. (2000). Prediction of slug liquid holdup: horizontal to upward vertical flow. International Journal of Multiphase Flow, 26(3):517 – 521.

[Grimholt and Skogestad, 2015] Grimholt, C. and Skogestad, S. (2015). 2nd ifac workshop on automatic control in offshore oil and gas production oogp 2015 optimization of oil field production under gas coning conditions using the optimal closed-loop estimator. IFAC-PapersOnLine, 48(6):39 – 44.

[Gulf Island Fabrication, nd] Gulf Island Fabrication (n.d.). Projects : Subsea. http://www.gulfisland.com/projects-subsea.php. Accessed: 2016-05-05.

[Haugen et al., 1995] Haugen, K., Kvernvold, O., Ronold, A., and Sandberg, R. (1995). Sand erosion of wear-resistant materials: Erosion in choke valves. Wear, 186:179–188.

[Huguenot Laboratories, nd] Huguenot Laboratories (n.d.). Metallurgical Analysis. https://www.huguenotlabs.com/shoppingcart/pages/Metallurgical-Analysis.html. Accessed: 20.05.2016.

[IEEE Globalspec, nd] IEEE Globalspec (n.d.). Trash pumps information.

[In Line Valve, nd] In Line Valve (n.d.). Control chokes. http://www.inlinevalve.co.uk/gneral_features.htm. Accessed: 2016-05-05.

[ISO, 2006] ISO (2006). Iso14224. petroleum, petrochemical and natural gas industries – collection and exchange of reliability and maintenance data for equipment.

[Johnson, 1995] Johnson, K. L. (1995). Contact mechanics and the wear of metals. Wear, 190(2):162–170.

[Johnson, 1998] Johnson, R. W. (1998). The Handbook of fluid dynamics. CRC Press, Boca Raton, Fla.

[Liu, 2015] Liu, F. (2015). Condition monitoring and prognosis for subsea multiphase pump.

[Lotz and Postlethwaite, 1989] Lotz, U. and Postlethwaite, J. (1989). Erosion-corrosion in disturbed two phase liquid-particle flow.

[MAN Turbomachinery, nd] MAN Turbomachinery (n.d.). Axial Compressors. http://turbomachinery.man.eu/products/compressors/axial. Accessed: 2016-05-05.

[Mazumder et al., 2004] Mazumder, Q. H., Shirazi, S. A., McLaury, B. S., Shadley, J. R., and Rybicki, E. F. (2004). A mechanistic model to predict erosion in multiphase flow in elbows downstream of vertical pipes.

[McLaury and Shirazi, 2000] McLaury, B. S. and Shirazi, S. A. (2000). An alternate method to api rp 14e for predicting solids erosion in multiphase flow. Journal of Energy Resources Technology, Transactions of the ASME, 122(3):115–122.

[MHI Compressor Corporation, nd] MHI Compressor Corporation (n.d.). Single shaft Centrifugal Compressor (MAC). https://www.mhicompressor.com/en/products/mco/mac_index.html. Accessed: 2016-05-05.

[Ministry of Petroleum and Energy, 2013] Ministry of Petroleum and Energy (2013). Norway's oil history in 5 minutes. https://www.regjeringen.no/en/topics/energy/oil-and-gas/norways-oil-history-in-5-minutes/id440538/. Accessed: 07.06.2016.

[Mishra et al., 1997] Mishra, B., Al-Hassan, S., Olson, D. L., and Salama, M. (1997). Development of a predictive model for activation-controlled corrosion of steel in solutions containing carbon dioxide.

[Muhlbauer, 2004] Muhlbauer, W. K. (2004). Pipeline Risk Management Manual : Ideas, Techniques, and Resources. Pipeline Risk Management Manual - Ideas, Techniques, and Resources. Elsevier Science, Burlington, 3rd ed. edition.

[Natural Resources Canada, nd] Natural Resources Canada (n.d.). Air Compressor Types and Controls. http://www.nrcan.gc.ca/energy/products/reference/14970. Accessed: 2016-05-05.

[Norwegian Petroleum, 2015a] Norwegian Petroleum (2015a). Exports of oil and gas. http://www.norskpetroleum.no/en/production-and-exports/exports-of-oil-and-gas/. Accessed: 07.06.2016.

[Norwegian Petroleum, 2015b] Norwegian Petroleum (2015b). Fields. http://www.norskpetroleum.no/en/facts/fields/. Accessed: 07.06.2016.

[Oil & Gas Portal, nd] Oil & Gas Portal (n.d.). Subsea technology and equipments. http://www.oil-gasportal.com/subsea-technology-and-equipments/. Accessed: 15.04.2016.

[Okhovat et al., 2014] Okhovat, A., Heris, S., Asgarkhani, M., and Fard, K. (2014). Modeling and simulation of erosion–corrosion in disturbed two-phase flow through fluid transport pipelines. Arabian Journal for Science and Engineering, 39(3):1497–1505.

[Ossai, 2012] Ossai, C. I. (2012). Predictive modelling of wellhead corrosion due to operating conditions: A field data approach. 2012.

[Pantazolpoulos, 1994] Pantazolpoulos, M. S. (1994). Vortex-induced vibration parameters: critical review.

[Papavinasam, 2014] Papavinasam, S. (2014). Corrosion control in the oil and gas industry. Gulf Professional Publ., Amsterdam.

[Parsi et al., 2014] Parsi, M., Najmi, K., Najafifard, F., Hassani, S., McLaury, B. S., and Shirazi, S. A. (2014). A comprehensive review of solid particle erosion modeling for oil and gas wells and pipelines applications. Journal of Natural Gas Science and Engineering, 21:850 – 873.

[Peters, 2003] Peters, J. (2003). Assessment of valve failures in the offshore oil & gas sector.

[Peters, 2014] Peters, J. (2014). Erosion management - using erosion testing combined with erosion modelling.

[Polyprocessing, nd] Polyprocessing (n.d.). Benefits of A Ball Valve.

[Rambøll, nd] Rambøll (n.d.). Designing subsea pipelines. `https://issuu.com/ramboll/docs/designing_hpht_pipeline_revideret_2?e=4162991/14825329`. Accessed: 07.05.2016.

[Reinås, 2012] Reinås, L. (2012). Wellhead fatigue analysis - surface casing cement boundary condition for subsea wellhead fatigue analytical models.

[Salama, 2000] Salama, M. M. (2000). An alternative to api 14e erosional velocity limits for sand-laden fluids. Journal of Energy Resources Technology, 122(2):71.

[Salama and Venkatesh, 1983] Salama, M. M. and Venkatesh, E. S. (1983). Evaluation of api rp 14e erosional velocity limitations for offshore gas wells.

[Salik and Buckley, 1981] Salik, J. and Buckley, D. (1981). Effect of mechanical surface and heat treatments on erosion resistance.

[Shirazi et al., 1995] Shirazi, S. A., Shadley, J. R., McLaury, B. S., and Rybicki, E. F. (1995). A procedure to predict solid particle erosion in elbows and tees. Journal of Pressure Vessel Technology, 117(1):45–52.

[Shorts, nd] Shorts, M. (n.d.). Understanding check valves: Sizing for the application, not the line size.

[Sooraj and Radhakrishnan, 2013] Sooraj, V. S. and Radhakrishnan, V. (2013). Elastic impact of abrasives for controlled erosion in fine finishing of surfaces. Journal of Manufacturing Science and Engineering, Transactions of the ASME, 135(5).

[Srinivasan, 1996] Srinivasan, S. (1996). Prediction of corrosivity of co2/h2s production environments.

[Subsea World News, 2013a] Subsea World News (2013a). GE Oil & Gas Launches New Subsea Manifold Design and Delivery Strategy. https://subseaworldnews.com/2013/09/04/ge-oil-gas-launches-new-subsea-manifold-design-and-delivery-strategy. Accessed: 2016-05-05.

[Subsea World News, 2013b] Subsea World News (2013b). South Stream: Construction of First Offshore Pipeline to Start in 2014. http://subseaworldnews.com/2013/07/05/south-stream-construction-of-first-offshore-pipeline-to-start-in-2014/. Accessed: 2016-05-05.

[Subsea World News, 2014] Subsea World News (2014). VIDEO: Technip Hybrid Umbilical for Chevron's Alder. https://subseaworldnews.com/2014/11/12/video-technip-hybrid-umbilical-for-chevrons-alder/. Accessed: 2016-05-04.

[Sundararajan and Shewmon, 1982] Sundararajan, G. and Shewmon, P. G. (1982). A new model for the erosion of metals at normal incidence.

[Sunnda Corporation, nd] Sunnda Corporation (n.d.). Ram Blowout Preventers (API-16A). http://www.blowout-preventers.com/ram-blowout-preventers.php. Accessed: 2016-05-05.

[Tipvalve Industrial Group, nd] Tipvalve Industrial Group (n.d.). Wellhead christmas tree. http://www.ball-valve-china.com/productsdetail/wellhead-valve/wellhead-christmas-tree/wellhead-christmas-tree/467.html. Accessed: 15.04.2016.

[Wada and Watanabe, 1987] Wada, S. and Watanabe, N. (1987). Solid particle erosion of brittle materials (part 3). Journal of the Ceramic Association, Japan, 95(1102):573–578.

[Zhang et al., 2003] Zhang, H.-Q., Wang, Q., Sarica, C., and Brill, J. P. (2003). Unified model for gas-liquid pipe flow via slug dynamics—part 1:

Model development. Journal of Energy Resources Technology, 125(4):266–273.

[Zhang and Chen, 2007] Zhang, Z. and Chen, Q. (2007). Comparison of the eulerian and lagrangian methods for predicting particle transport in enclosed space.

A Tables

A.1 A complete list of sand erosion parameters

Table A.1: A complete list of the physical parameters important in the modelling of sand erosion, taken from the review by Parsi et al. [Parsi et al., 2014]

Parameters
Critical friction coefficient
Critical Poision coefficient
Critical strain
Cutting energy
Deformation energy
Depth of deformation
Enthalpy of melting
Erosion resistance
Flow stress
Fracture thoughness
Friction coefficient
Grain mass
Grain molecular weight
Heat capacity
Impact angle
Impact angle max wear
Incremental strain per impact
KE transfer from particle to target
Melting temperature
Moment of intertia
Number of impacts
Particle density
Particle size
Particle velocity
Poisson coefficient
Pressure
Rebound velocity
Roundness
Strain hardening
Target density
Target hardness
Temperature
Thermal conductivity
Young modulus

A.2 Factors for the McLaury and Shirazi (2000) model

Table A.2: Sand sharpness factors, F_S [McLaury and Shirazi, 2000].

Description	F_S [-]
Rounded, spherical glass beads	0.20
Semi-rounded, rounded corners	0.53
Sharp corners, angular	1.00

Table A.3: Shape and penetration factors [McLaury and Shirazi, 2000]

Shape	L_0 [mm]	F_P [mm/kg]
Elbow (90)	30	206
Tee	27	206

A.3 Material properties for the DNV-GL (2015) model and the Haugen et al. (1995) model

Table A.4: Material properties for some selected materials, used in the sand erosion model by DNV-GL. For a complete table, see page 23 in "Managing sand production and erosion" [DNV-GL, 2015b].

Material	Description	ρ_t [kg/m^3]	K [(m/s)$^{-n}$]	n
Carbon Steel	Ductile	7 800	2.00E-09	2.6
SS316	Ductile	8 000	2.00E-09	2.6
HDPE	Ductile	1 150	3.50E-09	2.9
Aluminium	Ductile	2 700	5.80E-09	2.3
Zirconia, PSZ	Brittle	5 700	4.10E-09	2.5
Tungsten Carbide, DC-05	Brittle	15 250	1.10E-10	2.3
Titanium Diboride. TiB2	Brittle	4 520	9.30E-09	1.9
Silicon Carbide, SiC	Brittle	3 100	6.50E-09	1.9
Ceramic Silicon Carbide, SiSiC	Brittle	3 100	7.40E-11	2.7

A.4 Parameters for the Haugen et al. (1995) model

Table A.5: The parameters used to calculate $F(\alpha)$ in Equation (3.104) taken from "Sand erosion of wear-resistant materials: Erosion in choke valves" by Haugen et al. [Haugen et al., 1995].

Constant	Value
A_1	9.370
A_2	42.295
A_3	110.864
A_4	175.804
A_5	170.137
A_6	98.298
A_7	31.211
A_8	4.170

A.5 Various factors known to affect corrosion

Table A.6: A list of the various form of corrosion [Papavinasam, 2014]

Corrosion mechanism
General corrosion
Galvanic corrosion
Pitting corrosion
Intergranular corrosion
Selective leaching
Crevice corrosion
Deposition corrosion
Cavitation corrosion
Fretting corrosion
Underdeposit corrosion
Microbiologically influenced corrosion
High temperature corrosion
Stress corrosion cracking (SCC)
Sulfide stress cracking (SSC)
Stray current corrosion
Alternating current corrosion
Corrosion under protective coating
Corrosion under insulation
Top-of-the-line corrosion (TLC)

A.6 Parameters for the Ossai (2012) model

Table A.7: The parameters used to calculate corrosion rate of the wellhead in the model by Ossai [Ossai, 2012].

Variable	Value [-]
α_{11}	-0.4508
α_{21}	-0.0009
α_{31}	-0.0261
α_{41}	0.0701
β_{11}	0.0038
β_{22}	0.997
β_{13}	0.2379
β_{14}	0.0597
β_{21}	0.0041
β_{22}	0.948
β_{23}	0.2323
β_{31}	0.003196
β_{32}	0.8196
β_{33}	1.3327
β_{41}	0.0051
β_{42}	0.7973

A.7 Results from parameter study

A.7.1 Parameter: Q_{L1}

Table A.8: The estimated erosion rates in mm/year of the components in the case study at different liquid velocities in m^3/s in Flow 1, Q_{L1}. The values were calculated by a variation of the MATLAB script in Appendix C.4.

Q_{L1}	Elbow 1	Elbow 2	Elbow 3	Choke 1	Choke 2
0.1	0	0.2095	0.0165	0.9030	0.4493
0.2	0.0267	0.2095	0.0823	0.9972	0.4993
0.3	0.2631	0.2095	0.2194	1.1916	0.5493
0.4	0.8077	0.2095	0.4353	1.4507	0.5993
0.5	1.6658	0.2095	0.4708	1.7667	0.6493
0.6	2.8239	0.2095	1.1051	2.1385	0.6993
0.7	4.2672	0.2095	1.5566	2.5668	0.7493
0.8	5.9812	0.2095	2.0832	3.0536	0.7993
0.9	7.9545	0.2095	2.6829	3.6010	0.8493
1.0	10.1769	0.2095	3.3537	4.2112	0.8993

Table A.9: The estimated lifetime in years of the components in the case study at different liquid velocities in m^3/s in Flow 1, Q_{L1}. The values were calculated by a variation of the MATLAB script in Appendix C.4.

Q_{L1}	Elbow 1	Elbow 2	Elbow 3	Choke 1	Choke 2
0.1	-	48	605	12	23
0.2	374	48	122	11	23
0.3	39	48	46	9	23
0.4	13	48	23	7	23
0.5	7	48	14	6	23
0.6	4	48	10	5	23
0.7	3	48	7	4	23
0.8	2	48	5	4	23
0.9	2	48	4	3	23
1.0	1	48	3	3	23

A.7.2 Parameter: Q_{G1}

Table A.10: The estimated erosion rates in mm/year of the components in the case study at different gas velocities in m^3/s in Flow 1, Q_{G1}. The values were calculated by a variation of the MATLAB script in Appendix C.4.

Q_{G1}	Elbow 1	Elbow 2	Elbow 3	Choke 1	Choke 2
0.1	0	0.2095	0.0060	0.0235	0.4493
0.2	0	0.2095	0.0082	0.0927	0.4493
0.3	0	0.2095	0.0107	0.2412	0.4493
0.4	0	0.2095	0.0136	0.5009	0.4493
0.5	0	0.2095	0.0165	0.9030	0.4493
0.6	0	0.2095	0.0200	1.4780	0.4493
0.7	0	0.2095	0.0238	2.2554	0.4493
0.8	0	0.2095	0.0278	3.2638	0.4493
0.9	0	0.2095	0.0321	4.5308	0.4493
1.0	0.0005	0.2095	0.0360	6.0834	0.4493

Table A.11: The estimated lifetime in years of the components in the case study at different gas velocities in m^3/s in Flow 1, Q_{G1}. The values were calculated by a variation of the MATLAB script in Appendix C.4.

Q_{G1}	Elbow 1	Elbow 2	Elbow 3	Choke 1	Choke 2
0.1	-	48	1662	426	23
0.2	-	48	1221	108	23
0.3	-	48	934	42	23
0.4	-	48	738	20	23
0.5	-	48	605	12	23
0.6	-	48	500	7	23
0.7	-	48	421	5	23
0.8	-	48	360	4	23
0.9	743731	48	312	3	23
1.0	21632	48	278	2	23

A.7.3 Parameter: Q_{L2}

Table A.12: The estimated erosion rates in mm/year of the components in the case study at different liquid velocities in m^3/s in Flow 2, Q_{L2}. The values were calculated by a variation of the MATLAB script in Appendix C.4.

Q_{L2}	Elbow 1	Elbow 2	Elbow 3	Choke 1	Choke 2
0.1	0	0	0	0.9030	0.2412
0.2	0	0.0016	0.0003	0.9030	0.3230
0.3	0	0.2095	0.0165	0.9030	0.4493
0.4	0	0.7245	0.0823	0.9030	0.6153
0.5	0	1.5627	0.2194	0.9030	0.8223
0.6	0	2.7076	0.4353	0.9030	1.0729
0.7	0	4.1418	0.7308	0.9030	1.3698
0.8	0	5.8497	1.1051	0.9030	1.7160
0.9	0	7.8188	1.5566	0.9030	2.1143
1.0	0	10.0381	2.0832	0.9030	2.5675

Table A.13: The estimated lifetime in years of the components in the case study at different liquid velocities in m^3/s in Flow 2, Q_{L2}. The values were calculated by a variation of the MATLAB script in Appendix C.4.

QL2	Elbow 1	Elbow 2	Elbow 3	Choke 1	Choke 2
0.1	-	-	-	12	42
0.2	-	861	35184	12	31
0.3	-	48	605	12	23
0.4	-	14	122	12	17
0.5	-	7	46	12	13
0.6	-	4	23	12	10
0.7	-	3	14	12	8
0.8	-	2	10	12	6
0.9	-	2	7	12	5
1.0	-	1	5	12	4

A.7.4 Parameter: Q_{G2}

Table A.14: The estimated erosion rates in mm/year of the components in the case study at different gas velocities in m^3/s in Flow 2, Q_{G2}. The values were calculated by a variation of the MATLAB script in Appendix C.4.

Q_{G2}	Elbow 1	Elbow 2	Elbow 3	Choke 1	Choke 2
0.1	0	0.1571	0.0107	0.9030	0.1113
0.2	0	0.1831	0.0136	0.9030	0.2406
0.3	0	0.2095	0.0165	0.9030	0.4493
0.4	0	0.2363	0.0200	0.9030	0.7590
0.5	0	0.2631	0.0238	0.9030	1.1916
0.6	0	0.2899	0.0278	0.9030	1.7696
0.7	0	0.3165	0.0321	0.9030	2.5152
0.8	0	0.3428	0.0360	0.9030	3.4508
0.9	0	0.3689	0.0408	0.9030	4.5988
1.0	0	0.3946	0.0458	0.9030	5.9814

Table A.15: The estimated lifetimes in year of the components in the case study at different gas velocities in m^3/s in Flow 2, Q_{G2}. The values were calculated by a variation of the MATLAB script in Appendix C.4.

Q_{G2}	Elbow 1	Elbow 2	Elbow 3	Choke 1	Choke 2
0.1	-	64	934	12	90
0.2	-	55	738	12	42
0.3	-	48	605	12	23
0.4	-	43	500	12	14
0.5	-	39	421	12	9
0.6	-	35	360	12	6
0.7	-	32	312	12	4
0.8	-	30	278	12	3
0.9	-	28	249	12	3
1.0	-	26	219	12	2

B Derivation of the particle equation of motion

A good place to begin is Newtons 2. law, which states that the sum of the forces F equals the mass of the object, m, multiplied with the acceleration of the object, a.

$$\sum F = m \cdot a \tag{B.1}$$

Forces acting on a particle is typically the gravitational force, the bouyancy force and the drag force. In this case only the drag force, F_D, is considered:

$$m \cdot a = F_D \tag{B.2}$$

The drag force on a particle in flow can be written as

$$F_D = 0.5\rho_f(V_f - V_p)|V_f - V_p|C_D A \tag{B.3}$$

where ρ_f is the fluid density, V_f is the fluid velocity, V_p is the particle velocity, C_D is the drag coefficient and A is the surface area of the particle [Johnson, 1998].The surface area, A, can be written as:

$$A = \pi r^2 = \pi \left(\frac{d_p}{2}\right)^2 = \frac{\pi d_p^2}{4} \tag{B.4}$$

and the acceleration, a, can be written as:

$$a = \frac{dv}{dt} = \left(\frac{dx}{dt} \cdot \frac{dv}{dx}\right) = v \cdot \frac{dv}{dx} \tag{B.5}$$

This gives the following equation:

$$mV_p \frac{dV_p}{dx} = 0.5\rho_f(V_f - V_p)|V_f - V_p|C_D \frac{\pi d_p^2}{4} \tag{B.6}$$

which is the same equation that is given in the article by Shirazi

C MATLAB scripts

C.1 Main script

```
clear all
close all
clc

parameters

%% Calculate Flow 3
p.Q3.l = p.Q1.l+p.Q2.l; % Liquid volumetric flow [m3/s]
p.Q3.g = p.Q1.g+p.Q2.g; % Gas volumetric flow [m3/s]
p.w3 = p.w1+p.w2; % Sand production rate [m3/s]

%% Calculation of the erosion in the bends
[ER.bend1 p] = bend(p.Q1.l, p.Q1.g, p.D1, p.w1, p); % Erosion...
    rate bend 1 [mm/year]
[ER.bend2 p] = bend(p.Q2.l, p.Q2.g, p.D1, p.w2, p); % Erosion...
    rate bend 2 [mm/year]
[ER.bend3 p] = bend(p.Q3.l, p.Q3.g, p.D2, p.w3, p); % Erosion...
    rate bend 3 [mm/year]

%% Erosion in choke valve 1 and 2
[ER.choke1 p] = choke(p.Q1.l, p.Q1.g, p.w1, p);
[ER.choke2 p] = choke(p.Q2.l, p.Q2.g, p.w2, p);

%% Initial wall thickness
bend1(1) = 10; % Initial wall thickness [mm]
bend2(1) = 10; % Initial wall thickness [mm]
bend3(1) = 10; % Initial wall thickness [mm]
choke1(1) = 10;
choke2(1) = 10;

n = 30; % Time scope [year]

for i = 2:n+1
    bend1(i) = bend1(i-1)-ER.bend1;
    bend2(i) = bend2(i-1)-ER.bend2;
    bend3(i) = bend3(i-1)-ER.bend3;
    choke1(i) = choke1(i-1)-ER.choke1;
    choke2(i) = choke2(i-1)-ER.choke2;
end

%% The plot
plot(0:n, bend1, 0:n, bend2, 0:n, bend3, 0:n, choke1, 0:n, ...
    choke2)
```

```
40 title('Basic case: system erosion', 'FontSize', 14)
41 xlim([0 n])
42 ylim([0 10])
43 xlabel('Time [year]')
44 ylabel('Wall thickness [mm]')
45 legend('Elbow 1', 'Elbow 2', 'Elbow 3', 'Choke 1' , 'Choke 2'...
       )
46
47 ER
```

C.2 Calculating erosion in a choke valve

```
1  function [ER p] = choke(Q_l, Q_g, w, p)
2      %% Parameters
3      C_unit = 1000*3600*24*365; % Conversion factor [m/s] to [...
           mm/year]
4      C1 = 1.25; % Geometry factor [-]
5      K = 2e-9; % Material erosion constant [(m/s)^-n]
6      rho_t = 7800; % Densiy carbon steel [kg/m3]
7      n = 2.6; % [-]
8      GF = 2; % Geometry factor
9      A_g = 2*p.choke.H*p.choke.D; % Effective gallery area [m2...
           ]
10     m_p = w*p.rho.p; % Mass rate of sand [kg/s]
11     D = p.D1*2.54/100; % Diameter from [inches] to [m]
12
13     %% Calculate mixing properties
14     A2 = (pi*D^2)/4; % Pipe cross sectional area [m2]
15     V.sl = Q_l/A2; % Superficial liquid velocity [m/s]
16     V.sg = Q_g/A2; % Superficial gas velocity [m/s]
17     rho.m = (p.rho.l*V.sl + p.rho.g*V.sg)/(V.sl+V.sg); % ...
           Mixture density [kg/m3]
18     mu.m = (p.mu.l*V.sl + p.mu.g*V.sg)/(V.sl+V.sg); % Mixture...
            viscosity [kg/ms]
19
20     Q.m = Q_l + Q_g; % Mixed volumetric flow
21     V.m = 0.75*Q.m/A_g; % Particle impact velocity
22
23     %% Calculate characteristic impact angle
24     alpha = atan(1/sqrt(2*p.choke.r)); % Particle impact ...
           angle [rad]
25     F = @(alpha) 0.6*(sin(alpha)+7.2* (sin(alpha)-(sin(alpha)...
           )^2)^0.6*(1-exp(-20*alpha)));
26
27     %% Calculate dimensionless parameters A and beta
28     A = rho.m^2*tan(alpha)*V.m*p.D1/(p.rho.p*mu.m); % [-]
29     beta = p.rho.p/rho.m; % [-]
30
```

```
31      %% Calculate the particle size correction function
32      gamma_c = 1/(beta*(1.88*log(A)-6.04));
33
34      if gamma_c > 0.1
35          gamma_c = 0.1;
36      end
37
38      gamma = p.d_p/p.D1;
39
40      if gamma < gamma_c
41          G = gamma/gamma_c;
42      else
43          G = 1;
44      end
45
46      %% Calculate erosion rate
47      ER = K*F(alpha)*V.m^n*G*C1*GF*m_p*C_unit/(rho_t*A_g); % ...
            Erosion rate [mm/year]
48  end
```

C.3 Calculating erosion in a bend

```
1   function [ER p] = bend(Q_l, Q_g, D, W, p)
2       %% Step 1: Determine stagnation length, L
3       L0 = (1-1.27*atan(1.01*D^(-1.89))+D^0.129)*1.18; % ...
            Stagnation length [inches]
4       p.L = L0*2.54/100; % Stagnation length [inches] to [m]
5       D_m = D*2.54/100; % Diameter [inches] to [m]
6
7       %% Step 2: Determine flow velocity profile
8       A = (pi*D_m^2)/4; % Cross sectional area
9       V.sl = Q_l/A; % Superficial liquid velocity
10      V.sg = Q_g/A; % Superficial gas velocity
11
12      p.rho_m = (V.sl*p.rho.l)/(V.sg+V.sl)+(V.sg*p.rho.g)/(V.sl...
            +V.sg); % Micture density [kg/m3]
13      p.mu_m = (V.sl*p.mu.l)/(V.sg+V.sl)+(V.sg*p.mu.g)/(V.sl+...
            V.sg); % Mixture viscosity [kg/ms]
14
15      p.V_char = V.sl;
16
17      %% Step 3: Determine the particle impact velocity
18      [x,V_p] = ode45(@(x, V_p) dvdx(x, V_p, p), [0 1], 1);
19      V_p = V_p*p.V_char; % Vector of particle velocities from ...
            x = 0 to x = L
20      V_L = V_p(end); % Particle impact velocity [m/s]
21
22      if V_L < 0
```

```
23          V_L = 0;
24      end
25
26
27
28      %% Step 4: Determine the erosion rate
29      F_m = (1.95e-5)/(120^-0.59); % Material hardness factor ...
            CS [-]
30      F_s = 0.53; % Sharpness factor [-]
31      F_p = 206/1000; % Penetration factor [m/kg]
32      Dref = 1; % [inches]
33      r_c = 1.5; % [-]
34      F_rD = exp(-(0.1*(p.rho_m^0.4*p.mu_m^0.65)/(p.d_p^0.3)+0...
            .015*p.rho_m^0.25+0.12)*(r_c-1.5)); % Radius curvature...
             factor [-]
35
36      ER = F_m*F_s*F_p*F_rD*(W*V_L^1.73)*3600*24*365*1000/(D/...
            Dref)^2; % Erosion rate [mm/year]
37  end
```

C.4 Parameter study

```
1   clear all
2   close all
3   clc
4
5   parameters
6
7   %% Calculate Flow 3
8   p.Q3.l = p.Q1.l+p.Q2.l; % Liquid volumetric flow [m3/s]
9   p.Q3.g = p.Q1.g+p.Q2.g; % Gas volumetric flow [m3/s]
10  p.w3 = p.w1+p.w2; % Sand production rate [m3/s]
11
12  %% Initial wall thickness
13  bend1(1:10,1) = 10; % Initial wall thickness [mm]
14  bend2(1:10,1) = 10; % Initial wall thickness [mm]
15  bend3(1:10,1) = 10; % Initial wall thickness [mm]
16  choke1(1:10,1) = 10; % Initial wall thickness [mm]
17  choke2(1:10,1) = 10; % Initial wall thickness [mm]
18
19  %% Calculate the different erosion rates
20  t = 1; % counter
21  x = 0.1:0.1:1; % interval
22  for n = x % Liquid volumetric flow 1
23      p.Q3.l = n + p.Q2.l; % Liquid volumetric flow 3
24
25      [ER.bend1(t) p] = bend(n, p.Q1.g, p.D1, p.w1, p); % ...
            Erosion rate elbow 1 [mm/year]
```

```
26      [ER.bend2(t) p] = bend(p.Q2.l, p.Q2.g, p.D1, p.w1, p); % ...
           Erosion rate elbow 2 [mm/year]
27      [ER.bend3(t) p] = bend(p.Q3.l, p.Q3.g, p.D2, p.w3, p); % ...
           Erosion rate elbow 3 [mm/year]
28      [ER.choke1(t) p] = choke(n, p.Q1.g, p.w1, p); % Erosion ...
           rate choke 1 [mm/year]
29      [ER.choke2(t) p] = choke(p.Q2.l, p.Q2.g, p.w2, p); % ...
           Erosion rate choke 2 [mm/year]
30
31      t = t + 1;
32  end
33
34  j = 1; % Counter
35  f = 30; % Field lifetime
36
37  for i = 1:10
38      % Elbow 1
39      if ER.bend1(i) > 0 %% In case no/very little erosion --> ...
           never-ending while loop
40          while bend1(i,j) > 0
41              bend1(i,j+1) = bend1(i,j) - ER.bend1(i); % ...
                   calculating wall thickness
42              j = j + 1; % counting years
43          end
44          b1(i) = j-1;
45      else
46          b1(i) = nan;
47      end
48
49      j = 1;
50
51      % Elbow 2
52      if ER.bend2(i) > 0 %% In case no/very little erosion --> ...
           never-ending while loop
53          while bend2(i,j) > 0
54              bend2(i,j+1) = bend2(i,j) - ER.bend2(i); % ...
                   calculating wall thickness
55              j = j + 1; % counting years
56          end
57          b2(i) = j-1;
58      else
59          b2(i) = nan;
60      end
61
62
63      j = 1;
64
65      % Elbow 3
66      if ER.bend3(i) > 0 %% In case no/very little erosion --> ...
```

```
        never-ending while loop
67          while bend3(i,j) > 0
68              bend3(i,j+1) = bend3(i,j) - ER.bend3(i); % ...
                    calculating wall thickness
69              j = j + 1; % counting years
70          end
71          b3(i) = j-1;
72      else
73          b3(i) = nan;
74      end
75
76      j = 1;
77
78      % Choke 1
79      if ER.choke1(i) > 0 %% In case no/very little erosion -->...
            never-ending while loop
80          while choke1(i,j) > 0
81              choke1(i,j+1) = choke1(i,j) - ER.choke1(i); % ...
                    calculating wall thickness
82              j = j + 1; % counting years
83          end
84          c1(i) = j-1;
85      else
86          c1(i) = nan;
87      end
88
89      j = 1;
90
91      % Choke 2
92      if ER.choke2(i) > 0 %% In case no/very little erosion -->...
            never-ending while loop
93          while choke2(i,j) > 0
94              choke2(i,j+1) = choke2(i,j) - ER.choke2(i); % ...
                    calculating wall thickness
95              j = j + 1; % counting years
96          end
97          c2(i) = j-1;
98      else
99          c2(i) = nan;
100     end
101
102     j = 1;
103 end
104
105 plot(x, b1, x, b3, x, c1)
106 xlabel('Liquid velocity in Flow 1 [m3/s]')
107 xlim([0.1 1])
108 ylim([0 f])
109 ylabel('Estimated lifetime [years]')
```

```
110 title('Effect of QL1 on estimated equipment lifetime', '...
       FontSize', 14)
111 legend('Elbow 1', 'Elbow 3', 'Choke 1')
```